Efficiently Computing First Passage Probabilities Using First Passage Capacities

Jackson Loper*

Data Science Institute, Columbia University, New York, NY, USA

Guangyao Zhou* and Stuart Geman

Division of Applied Mathematics, Brown University, Providence, RI, USA

(Dated: December 18, 2019)

A reversible stochastic differential equation is initialized at position x_0 – where will it go next? What is the probability it will reach one region before it reaches another region? We here propose an approach for estimating the probability that a given target, among many, will be the first to be reached by a reversible stochastic differential equation. We focus on the situation that it takes a long time to hit any target; in this case direct simulation of the hitting probabilities becomes prohibitively expensive. We turn this curse into a blessing; if the timescales are sufficiently long the system will essentially "forget" its initial condition before it hits any target. In this case we show that the hitting probabilities can be accurately approximated using only local simulations around each target, obviating the need for global simulations. Numerical experiments on idealized energy landscape show the estimates can be nearly as accurate as direct simulations and thousands of times faster to compute.

* These two authors contributed equally

I.   Introduction

Reversible diffusions play a key role in a wide variety of physical systems. For example, the folding of macromolecules into their native configurations is often posed as a diffusion (either directly through simulations of atomic dynamics or indirectly through mesoscopic models [1–3]), the fluctuation of chemical species in solution can be modeled as diffusions ("chemical Langevin equations" are one classic example of this approach [4, 5]), the motion of particles through membranes can be posed as a diffusion [6], and so-on. In all cases, the evolution of the physical state of the system at time t is represented through a variable X_t, and this variable evolves according to a stochastic differential equation.

In this paper we seek to estimate first-passage hitting probabilities of such diffusions: given an initial condition X_0 and two targets, A, B, what is the probability that we will hit target A first? Here each target represents a set of physical configurations. For example, if X represents the position of a particle trapped inside a sphere with two holes, A and B might represent the two holes. The hitting probability then indicates the probability that the particle exits through the first hole. This probabilities are also sometimes called "splitting probabilities" [7]. This work develops a new algorithm for approximating these hitting probabilities.

The proposed algorithm will not be useful for every diffusion; it is designed for cases where the diffusion can "forget" its initial condition before either target is hit. To make this idea rigorous, we need three ingredients:

- the initial configuration lies inside M, a set of physical configurations

- the targets A and B lie outside the set M

- the first passage time out of M is long (a long time elapses before the process exits the set M)

This last condition is vague – how long is long enough? A simplistic answer is that the algorithm will be more accurate when the first passage time is longer. A more precise answer requires some machinery from the theory of ergodicity. Recall that reversible diffusions are ergodic: as time goes on, it gets harder and harder to guess the initial condition from it's final configuration. If the first passage time out of M is long enough, it therefore follows that

the hitting probability will be nearly the same no matter which initial condition we started from. It is this property we actually need: if the hitting probability varies by at most ε among all initial conditions inside the set M, the proposed algorithm's approximation error is less than $\sqrt{2\varepsilon}$. Figure 1 gives a rough sketch of this idea. A rigorous definition is given in §II.

Many standard methods for calculating hitting probabilities fail in exactly the cases where the proposed algorithm excels. When the escape time from M is large, the associated partial differential equations often include large Lipschitz constants, and direct Monte-Carlo simulation requires prohibitive number of timesteps (cf. [8–10]). Some authors take a pessimistic view on this subject: "If these processes are intrinsically slow, i.e. require an extensive sampling of state space, not much can be done to speed up their simulation without destroying the dynamics of the system" [11].

In fact, some kind of separation of timescales can make analysis easier. The literature includes a variety of tools which use this idea to advantage. Here we review a few of these tools:

Asymptotic analyses: When the targets are very small, the first passage hitting times are often well-approximated by asymptotic formulae. The "narrow-escape problem" (NEP) is a prototypical example; X is a Brownian motion trapped inside a set by reflecting boundaries, and the targets are very small windows in boundary of the sphere. A similar problem arises when determining the chance that a particle will escape to infinity instead of being captured by a local attractor (this is mathematically equivalent to what is sometimes called the "competitive effects of reaction-diffusion controlled equations" cf. [12, 13]). Much of this literature focuses on making these formulas as accurate as possible for specific geometric configurations, such as the case of N circular targets (cf. [14]), the case that one targets lie at the end of a long tube (cf. [15]), and the case that the motion is trapped inside a symmetric domain (cf. [16–19]). There is also some work on efficient numerical methods for low-dimensional problems (cf. [20]). Note that in these asymptotic limits the first-passage probabilities are inversely proportional to the mean first-passage times, so all of these techniques allow us to estimate first-passage probabilities.

Markov State Models: Markov State Models (MSM) begin by partitioning the state-

space of the diffusion into n sets ("states"). The diffusion can be understood at a coarse level by looking at which state the process is in at any given time (cf. [21–23]). If this coarse process is approximately Markovian, we can simulate the discrete process as long as we know the distribution on the exit times and the probability of transitioning to each possible state. The amount of computational time required to simulate from this approximate process does not depend upon how long the process actually spends in each state. This allows one to overcome the challenges of long time-scales.

Site-localizing functions: Site-localizing functions take a relaxed version of the MSM idea; instead of creating a hard partitioning the space, one constructs basis functions $g_1(x) \cdots g_n(x)$ such that $\sum_i g_i(x) = 1$. In many cases the action of the relevant infinite-dimensional diffusion operators can be well-approximated by the their action on the n-dimensional space spanned by these basis functions. For example, under a separation-of-timescales assumption, Morro (cf. [24]) shows a way to design basis functions which faithfully represent the diffusion's behavior on the slow timescale.

Milestoning: In some cases it is possible to construct a low-dimensional reaction coordinate which measures the distance from the targets in some suitable metric. The dynamics of the diffusion along this coordinate are generally non-Markovian, but nonetheless they can be approximated with a low-dimensional stochastic differential equation. If the reaction coordinate is carefully chosen, many properties of the original diffusion are maintained in this one-dimensional projection [7]. Simulating from this low-dimensional approximate diffusion can yield useful insight into the overall behavior [25]. This is especially true of the system mixes quickly within the level-sets of the reaction coordinate. Otherwise, an accurate estimate can still be obtained by subdividing the level-sets of the reaction coordinate and tracing individual trajectories between these subdivisions; this idea leads to techniques such as "Milestoning without a reaction coordinate" (cf. [26]).

Here we investigate a different approach, using the fact that a diffusion eventually forgets its initial condition; we give an overview of the main idea here. Let $h(x)$ denote the hitting probability when the diffusion is initialized at x. If the diffusion nearly forgets its initial condition in M before it hits either target, it follows that $|h(x) - h(y)| < \varepsilon \ll 1$ for

every $x, y \in M$. We then recall that h can be understood as the solution of a variational problem (we give review of this matter in Appendix A); this suggests we might try to solve the associated variational problem subject to the hard constraint that $\varepsilon = 0$, i.e. there is some unknown constant $\bar{h}$ such that $h(x) = \bar{h}$ for every $x \in M$. We could then solve the constrained variational problem and calculate $\bar{h}$. In Theorem 1, we bound the error introduced by this approximation: $|\bar{h} - h(x)| \leq \sqrt{2\varepsilon}$. Moreover, under this approximation the calculation of $\bar{h}$ becomes much easier; $\bar{h}$ only on the dynamics outside of M, and this dependency can be summarized through what we call "first passage capacities."

This approach can get accurate results while completely ignoring all dynamics inside M. This is particularly valueable if M is a large, high-dimensional set. When M is very large, it is unclear how one would partition M, making Markov State Models difficult to implement. Similarly it is unclear how one should formulate a reaction coordinate, making milestoning approaches difficult to implement. Integrating over all of M is computationally burdensome in this case, making site-localizing functions difficult to implement. Asymptotic techniques from the narrow escape/reaction-controlled diffusion literature may still be applied, but only if the problem falls into one of the very specific cases which have already been studied. Most of these cases lie in two or three-dimensions, feature regular targets, and assume the diffusion is has no energetic potential. By contrast, first passage capacities can be calculated efficiently for a diffusion with an arbitrary energetic potential, target shape, and ambient dimension. Moreover, first-passage capacities are a fundamentally non-asymptotic technique; for any problem the approximation error is bounded explicitly in terms of the extent to which the hitting probability varies inside M, i.e. ε. First-passage capacities do come with a significant limitation, however: they do not give direct insight into the overall timescale of the diffusion. There is an overall proportionality constant which connects first-passage hitting probabilities to the first-passage hitting times, and this constant cannot be recovered from the first-passage capacities. We discuss this limitation further in §VI.

In the following section (§II, "Preliminaries") we will introduce notation, define our diffusion, define first passage hitting probabilities, define our main assumption, and finally define the first-passage capacities that are at the heart of this approach. In §III we show that these capacities can be used to accurately estimate first-passage probabilities as long as our assumption holds; we also give an example where this condition is guaranteed. In §IV, we develop an approach to computing the first passage capacities. In §V we look at the results
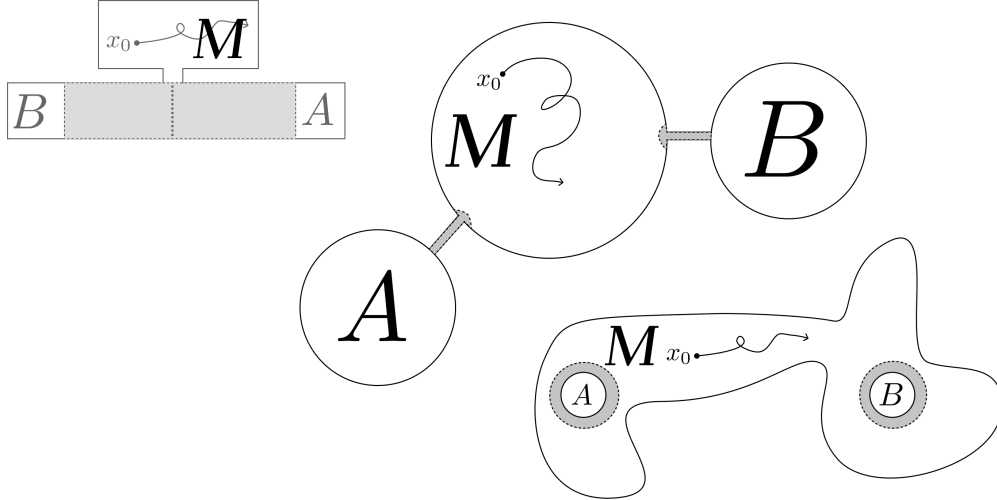
Figure 1. **First passage capacities allow efficient computation of hitting probabilities.** We consider a reversible stochastic differential equation in an n-dimensional state-space. Let us say we initialize the diffusion at some configuration x_0 inside the set M; what is the probability it will reach region A first before B? We assume that the hitting probability is nearly the same for every initial condition $x_0 \in M$ (it must differ by at most ε among all such initial conditions). Theorem 1 then shows that the hitting probability can then be approximated to within $\sqrt{2\varepsilon}$ using only "first passage capacities." These capacities can be computed using only simulations that take place outside of M. Above we sketch several examples where the condition can hold. In each case, the first passage capacities can be computed using simulations performed in the gray areas.

of computational experiments on a five-dimensional diffusion.

II. Preliminaries

Let us first define our diffusion process. Our results are about diffusion process X confined to an open bounded set $\Omega \subset \mathbb{R}^n$ with reflecting smooth boundary $\partial\Omega$ for $n \geq 3$. We assume X is driven by an n-dimensional standard Brownian motion W, i.e.

$$\mathrm{d}X_t = b(X_t)\mathrm{d}t + \sigma(X_t)\mathrm{d}W_t \tag{1}$$

where $b : \Omega \to \mathbb{R}^n$ and $\sigma : \Omega \to \mathbb{R}^{n \times n}$ are continuously differentiable vector-valued and matrix-valued functions. We further assume that $a(x) = \sigma(x)\sigma(x)^T$ is uniformly elliptic on Ω, i.e. the smallest eigenvalues of a are bounded away from zero. Let $\bar{\Omega}$ denote the closure of Ω (and in general let $\bar{S}$ denote the closure of any set $S \subset \bar{\Omega}$). For the precise definition of the reflected process, we adopt the framework developed by Lions and Sznitman[27]: Let

$\mathfrak{n} = \mathfrak{n}(x)$ denote the outward normal of $\partial\Omega$ and $\nu : \partial\Omega \to \mathbb{R}^n$ a smooth vector field satisfying $\mathfrak{n}^T\nu \geq c > 0$, and assume that $x_0 \in \Omega$. Then there is a unique pathwise continuous and W-adapted strong Markov process $X_t \in \bar{\Omega}$, and (random) measure L, such that

$$X_t = x_0 + \int_0^t b(X_s)ds + \int_0^t \sigma(X_s)dW_s - \int_0^t \nu(X_s)L(ds) \tag{2}$$

and $L(\{t : X_t \notin \partial\Omega\}) = 0$. For convenience, we will refer to X by simply saying "the reflected diffusion process (1)." We further assume that X is a reversible process, with equilibrium distribution given by

$$\rho(x) \doteq \frac{1}{Z}e^{-U(x)} \quad Z = \int_{x\in\Omega} e^{-U(x)}dx$$

where $U : \bar{\Omega} \to \mathbb{R}$ is continuously differentiable. As shown by Chen[28], to ensure that X is reversible it is sufficient that

$$b_i(x) = \frac{1}{2}\sum_j \partial a_{ij}(x)/\partial x_j - \frac{1}{2}\sum_j a_{ij}(x)\partial U(x)/\partial x_j$$
$$\nu(x) = a(x)\mathfrak{n}(x) \tag{3}$$

where $a(x) = \sigma(x)\sigma(x)^T$ is uniformly elliptic. When the conditions in (3) are in force we will say that X satisfies the reversibility conditions relative to U. We assume these conditions throughout the paper.

The main goal of this paper is to estimate first passage hitting probabilities for X. We here give a formal definition for these hitting probabilities:

Definition 1. *(First passage hitting probabilities). Fix two disjoint sets $A, B \subset \Omega$. The first-passage hitting probability function $h_{A,B}(x)$ indicates the probability that the process X visits A before B if it is initialized at $X_0 = x$. Formally,*

$$h_{A,B}(x) \triangleq \mathbb{P}(X_{\tau_{A\cup B}} \in A | X_0 = x)$$

where $\tau_{A\cup B}$ indicates the first passage time to $A \cup B$, i.e. $\tau_{A\cup B} \triangleq \inf\{t \geqslant 0 : X_t \in A \cup B\}$. Throughout this paper we will use τ_S to denote the first passage time to a set S and $h_{S,S'}$ to denote the hitting probability function for targets S, S'.

It turns out that these hitting probabilities are much easier to estimate if the process forgets its initial condition to such an extent that the hitting probabilities are nearly constant for any initial condition inside a set M:

Definition 2. *(The ε-flatness condition) A hitting probabiliy function $h_{A,B}(x)$ is said to be "ε-flat relative to M" whenever*

$$\sup_{x,y \in M} |h_{A,B}(x) - h_{A,B}(y)| < \varepsilon$$

The ε-flatness of $h_{A,B}$ is only a narrow view into the ergodicity of the process X. However it is exactly the view we need; the ε-flatness of $h_{A,B}$ gives us a way to quantify the extent of the equilibrium with respect to what we're interested in. As we shall see in Theorem 1, it is also exactly the condition we need to show that the hitting probabilities within M can be well-approximated using "first-passage capacities." These capacities are the last piece we must define:

Definition 3. *(Capacity) Let $S \subset \tilde{S} \subset \Omega$ be open sets and let X be a diffusion governed by the SDE in Equation (2) and satisfying the reversibility conditions in Equation (3). The first-passage capacity $\mathrm{cap}(S, \tilde{S})$ for X is defined as*

$$\mathrm{cap}(S, \tilde{S}) \triangleq \int_{\tilde{S} \setminus S} ||\sigma(x) \nabla h_{S, \tilde{S}^c}(x)||^2 e^{-U(x)} \mathrm{d}x$$

We refer the reader to Appendix A for more details on capacity and the related concept of Dirichlet form. Note that there are several related definitions of "capacity" in the probabilistic potential theory literature, all slightly different. For example, the Harmonic capacity arises by taking the above definition in the special case when the diffusion is a simple Brownian motion. This definition most closely follows the work of Bovier [29, 30]. Throughout this work, the term is used only in the sense of the above definition.

III. Main theoretical results

Our main theorem shows that the first-passage capacities gives accurate approximations of the hitting probabilities when the hitting probabilities are themselves ε-flat in a region outside a neighborhood of the targets.

Theorem 1. *Let $A \subset \tilde{A}, B \subset \tilde{B}$ be open sets and assume that $h_{A,B}(x)$ is ε-flat relative to $\Omega \backslash (\tilde{A} \cup \tilde{B})$. Then the first-passage probabilities are well-approximated by the first-passage capacities:*

$$\sup_{x \notin \tilde{A}, \tilde{B}} \left| h_{A,B}(x) - \frac{\operatorname{cap}(A, \tilde{A})}{\operatorname{cap}(A, \tilde{A}) + \operatorname{cap}(B, \tilde{B})} \right| \leqslant \varepsilon + \sqrt{\varepsilon/2}$$

We defer the proof to Appendix C. Note that the generalization to multiple targets is straightforward due to the additive property of capacities (Proposition 2 in Appendix A); if you have n targets and approximate the hitting probability to each by taking it to be proportional to the corresponding capacity, then all probabilities will be within $\varepsilon + \sqrt{\varepsilon/2}$ of the truth.

When might the ε-flatness condition hold? In the introduction, we gave an intuitive explanation for when this might be expected to happen, namely whenever the diffusion forgets its initial condition before it hits the targets. To prove the ε-flatness condition for a particular problem, one must make this idea rigorously. To offer the reader a flavor for how this may be done, we offer the following examples:

Theorem 2. *(Examples of ε-flatness). Let $\mathcal{B}(x, r) = \{y : \|x - y\| < r\}$ denote the ball of radius r centered at x.*

1. *Fix $r, \varepsilon > 0$. We can then find $\delta > 0$ with the following property. For any convex set Ω with diameter less than or equal to 1, any $x_A, x_B \in \Omega$, any diffusion such that $\nabla U(x) = 0$ for all $x \notin \mathcal{B}(x_A, \delta) \cup \mathcal{B}(x_B, \delta)$, and any $A \subset \mathcal{B}(x_A, \delta), B \subset \mathcal{B}(x_B, \delta)$, we have that $h_{A,B}$ is ε-flat on $\Omega \backslash \mathcal{B}(x_A, r) \cup \subset \mathcal{B}(x_B, r)$.*

2. *Fix $r, \varepsilon > 0$ and $r' < r$. We can then find n with the following property. For any convex set $\Omega \in \mathbb{R}^n$ with diameter less than or equal to 1, any x_A, x_B such that $\mathcal{B}(x_A, r), \mathcal{B}(x_B, r) \subset \Omega$, any diffusion such that $\nabla U(x) = 0$ for all $x \notin \mathcal{B}(x_A, r') \cup \mathcal{B}(x_B, r')$, and any $A \subset \mathcal{B}(x_A, r'), B \subset \mathcal{B}(x_B, r')$, we have that $h_{A,B}$ is ε-flat on $\Omega \backslash \mathcal{B}(x_A, r) \cup \subset \mathcal{B}(x_B, r)$.*

A proof can be found in Appendix B. The first example shows how hitting probabilities become flat as the targets become small. The second example notes that even if we fix the radius of the targets, the hitting probabilities becomes flat if the ambient dimension n is high. Both points can be proved by showing that the rate of ergodicity inside Ω is fast and it generally takes a long time to hit the targets.

IV.   Capacity Estimation

For a class of stochastic systems, characterized by a separation of time scales such that the process of finding targets is slow compared to the process of exploring the regions away from the targets, we have reduced the estimation of first-passage probabilities to the evaluation, or approximation, of capacities. Generically, given the process defined in Equation (1), satisfying the reversibility conditions in (3) relative to a continuously differentiable energy U, our goal is to evaluate

$$\text{cap}(A, \tilde{A}) = \int_{\tilde{A}\backslash A} ||\sigma(x)\nabla h_{A,\tilde{A}^c}(x)||^2 e^{-U(x)}\mathrm{d}x \tag{4}$$

for a target A and neighborhood $\tilde{A}$.

The calculation is local, in that $\text{cap}(A, \tilde{A})$ depends only on the behavior of U on $\tilde{A}\backslash A$, but it is not uncomplicated. We will propose here a Monte Carlo approach to evaluating the integral, made up of a combination of analytic reductions and highly orchestrated random walks. Inevitably, the effectiveness, or even feasibility, of the approach will depend on the particulars of the stochastic system, (1).

We begin by replacing the volume integral in (4) with a surface integral:

Proposition 1. *For any regions G and $\tilde{G}$ having smooth boundaries and such that $A \subset G \subset \tilde{G} \subset \tilde{A}$, $\text{cap}(A, \tilde{A},)$ can be expressed as a flux leaving $\tilde{G}\backslash G$:*

$$\text{cap}(A, \tilde{A}) = \int_{\partial(\tilde{G}\backslash G)} h_{A,\tilde{A}^c}(x)\mathfrak{n}(x)^T a(x)\nabla h_{G,\tilde{G}^c}(x)e^{-U(x)}\mathscr{H}(dx) \tag{5}$$

where $a(x) = \sigma(x)\sigma(x)^T$ is the diffusion matrix, $\mathscr{H}(dx)$ is the $(n-1)$-dimensional Hausdorff measure, and $\mathfrak{n}$ represents the outward-facing (relative to the set $\tilde{G}\backslash G$) normal vector on $\partial(\tilde{G}\backslash G)$.

This result is almost certainly already known; a formal proof is in Appendix D.

There is a great deal of freedom in choosing G and $\tilde{G}$; the idea is to choose them so as to make the surface integrals as simple as possible. Before pursuing this, we mention that there are many other ways to reduce the volume integral (4) to a flux integral, some of which might make more sense than (5) for a particular problem. Specifically, by a corollary

of Proposition (1), $\mathrm{cap}(A, \tilde{A})$ can be written as the flux of a different field, but this time through a single surface (see Appendix D):

Corollary 1. *For any region S having smooth boundary ∂S, and such that $A \subset S \subset \tilde{A}$, $\mathrm{cap}(A, \tilde{A},)$ can be expressed as a flux leaving S:*

$$\mathrm{cap}(A, \tilde{A}) = \int_{\partial S} \mathfrak{n}(x)^T a(x) \nabla h_{A,\tilde{A}^c}(x) e^{-U(x)} \mathcal{H}(dx) \tag{6}$$

where a and $\mathcal{H}(dx)$ are as defined in the Proposition, and $\mathfrak{n}$ is the outward-facing normal on ∂S.

The possible advantage is that there is only one surface and the integrand involves only one first-passage probability function, $h_{A,\tilde{A}^c}(x)$, instead of two. The possible disadvantage is the need to estimate $\nabla h_{A,\tilde{A}^c}$ on S, which is harder than estimating $h_{A,\tilde{A}^c}$. As we will see shortly, judicious choices for G and $\tilde{G}$ can mitigate, and in some cases even eliminate, the need to estimate gradients of first-passage probabilities.

Returning to the representation in (5), there are two surface integrals, each of which can be viewed as an expectation, as follows: Define a probability measure on ∂G by

$$\mathscr{P}(dx) \doteq \frac{1}{Z} e^{-U(x)} \mathcal{H}(dx) \text{ where } Z = \int_{\partial G} e^{-U(x)} \mathcal{H}(dx)$$

and define $\tilde{\mathscr{P}}(dx)$ and $\tilde{Z}$ analogously, but on $\partial \tilde{G}$ rather than ∂G. Then

$$\begin{aligned} \mathrm{cap}(A, \tilde{A}) &= \int_{\partial \tilde{G}} h_{A,\tilde{A}^c} \mathfrak{n}^T a \nabla h_{G,\tilde{G}^c} e^{-U} \mathcal{H}(dx) - \int_{\partial G} h_{A,\tilde{A}^c} \mathfrak{n}^T a \nabla h_{G,\tilde{G}^c} e^{-U} \mathcal{H}(dx) \\ &= Z \int_{\partial \tilde{G}} h_{A,\tilde{A}^c} \mathfrak{n}^T a \nabla h_{G,\tilde{G}^c} \tilde{\mathscr{P}}(dx) - Z \int_{\partial G} h_{A,\tilde{A}^c} \mathfrak{n}^T a \nabla h_{G,\tilde{G}^c} \mathscr{P}(dx) \end{aligned} \tag{7}$$

where, in these integrals, the normal, $\mathfrak{n}$, points outward from *both* G and $\tilde{G}$. If now $y_1, y_2, \ldots, y_m \sim$ iid $\mathscr{P}(dx)$, then

$$\frac{1}{m} \sum_{i=1}^{m} h_{A,\tilde{A}^c}(y_i) \mathfrak{n}^T(y_i) a(y_i) \nabla h_{G,\tilde{G}^c}(y_i) \overset{m \to \infty}{\longrightarrow} \int_{\partial G} h_{A,\tilde{A}^c} \mathfrak{n}^T a \nabla h_{G,\tilde{G}^c} \mathscr{P}(dx)$$

$$\text{and} \quad \frac{1}{m} \sum_{i=1}^{m} e^{U(y_i)} \overset{m \to \infty}{\longrightarrow} \int_{\partial G} e^{U} \mathscr{P}(dx) = \frac{|\partial G|}{Z}$$

where $|\partial G|$ is the surface area of G. Putting these together, we get the large n approximation

$$Z \int_{\partial G} h_{A,\tilde{A}^c} \mathfrak{n}^T a \nabla h_{G,\tilde{G}^c} \mathscr{P}(dx) \approx |\partial G| \frac{\sum_{i=1}^{m} h_{A,\tilde{A}^c}(y_i) \mathfrak{n}^T(y_i) a(y_i) \nabla h_{G,\tilde{G}^c}(y_i)}{\sum_{i=1}^{m} e^{U(y_i)}}$$

If we now extend all of this to $\partial \tilde{G}$, with $\tilde{y}_1, \tilde{y}_2, \ldots, \tilde{y}_n \sim$ iid $\tilde{\mathscr{P}}(dx)$, and put the approximations into (7), then for large n and m

$$\begin{aligned}
\text{cap}(A, \tilde{A}) \approx{} & |\partial \tilde{G}| \frac{\sum_{i=1}^{n} h_{A,\tilde{A}^c}(\tilde{y}_i) \mathfrak{n}^T(\tilde{y}_i) a(\tilde{y}_i) \nabla h_{G,\tilde{G}^c}(\tilde{y}_i)}{\sum_{i=1}^{n} e^{U(\tilde{y}_i)}} \\
& - |\partial G| \frac{\sum_{i=1}^{m} h_{A,\tilde{A}^c}(y_i) \mathfrak{n}^T(y_i) a(y_i) \nabla h_{G,\tilde{G}^c}(y_i)}{\sum_{i=1}^{m} e^{U(y_i)}}
\end{aligned} \tag{8}$$

To make this useful, we will need to choose G and $\tilde{G}$ so that (i) we can readily sample from $\mathscr{P}(dx)$ and $\tilde{\mathscr{P}}(dx)$; (ii) the surface areas $|\partial G|$ and $|\partial \tilde{G}|$ can be well approximated; (iii) the first-passage probability $h_{A,\tilde{A}^c}$ can be well approximated on G and $\tilde{G}$; and (iv) the gradient $\nabla h_{G,\tilde{G}^c}$ can also be well approximated on G and $\tilde{G}$. The first two of these challenges lend themselves to more-or-less routine, though not necessarily easy methods, including importance and rejection sampling. Of course we're free to choose G and $\tilde{G}$ to make (i) and (ii) as easy as possible.

As for approximating first-passage probabilities and their gradients, broadly speaking there are two approaches. It is well known that first-passage probabilities satisfy an elliptic PDE related to the infinitesimal generator—see Appendix A, Equation (A1)—and we could therefore choose from a selection of numerical solvers. One drawback with this approach is that numerical PDE methods are famously difficult to employ successfully in high dimensions ("curse of dimensionality"). Here, in a different direction, we exploit the connection between first-passage probabilities and the underlying random walk in order to develop Monte Carlo tools suitable for estimating both $h_{A,\tilde{A}^c}$ and $\nabla h_{G,\tilde{G}^c}$ on the surfaces ∂G and $\partial \tilde{G}$. These tools are based on what we will call the "shell method," which we describe briefly in the following paragraphs and in full detail in Appendix F.

Generically, given two simply-connected regions R and $\tilde{R}$, with $R \subset \tilde{R}$, and a set S such that $R \subset S \subset \tilde{R}$, we seek an approximation to the function $h_{R,\tilde{R}^c}$ on the surface ∂S. In principle, we could begin with a fine-grained partitioning of ∂S into simply-connected "cells," and for each cell run the diffusion X_t many times, recording whether or not the

path first exits $\partial(\tilde{R}\backslash R)$ at ∂R. The fraction of paths that first exit at ∂R constitutes an estimate of $h_{R,\tilde{R}^c}(x)$ for any x in the current cell. But this is wasteful and likely infeasible in all but the simplest of settings. Much of the waste stems from the fact that the ensemble of all paths generated from all cells will likely include many near collisions of paths scattered throughout $\partial(\tilde{R}\backslash R)$. An alternative, divide-and-conquer approach, is to introduce multiple sets, $S_0, S_1, \ldots, S_n$ such that

$$R = S_0 \subset \cdots \subset S_{m-1} \subset S_m = S \subset S_{m+1} \subset \cdots \subset S_n = \tilde{R}$$

and use sample paths from X, *locally*, to estimate the transition probability matrices from each cell within each "shell" ∂S_k to each cell of its neighboring shells, ∂S_{k-1} and ∂S_{k+1}. Equipped with these transition matrices, the first-passage probability for a given $x \in S$ is computed algebraically, without further approximation.

S must have been chosen not only to satisfy $R \subset S \subset \tilde{R}$ but also in such a way as to make it feasible to sample from ∂S under the probability measure $\frac{1}{Z}e^{-U}\mathscr{H}(dx)$. After that, $S_k\ k = 1, \ldots, n-1$ are chosen so that the shells nest and are in close proximity; the hitting times starting from a sample in ∂S_k and ending at $\partial S_{k-1} \cup \partial S_{k+1}$ must be short enough to encourage many repeated runs. The output is a set of samples, $z_1, \ldots, z_N \sim \frac{1}{Z}e^{-U}\mathscr{H}(dx)$ on ∂S together with the approximate value of $h_{R,\tilde{R}^c}(x)$ at each sample $x = z_i$. (In fact, though the main purpose is to estimate $h_{R,\tilde{R}^c}$ on ∂S, a byproduct is a sample from $\frac{1}{Z}e^{-U}\mathscr{H}(dx)$ on all of the shells ∂S_k, along with an estimate of $h_{R,\tilde{R}^c}$ at every sample.) With the choice of A for R and $\tilde{A}$ for $\tilde{R}$, the algorithm becomes directly applicable to the estimation of $h_{A,\tilde{A}^c}$ on ∂G and $\partial\tilde{G}$, taking $S = G$ in the former case and $S = \tilde{G}$ in the latter.

The shell method is closely related to milestoning[25, 31, 32] and Markov state models[21–23], though more tailored to the problem at hand. In particular, our interest here is in computing the first-passage probabilities rather than in approximating the underlying process. Also, the discretizations of the shells are *adaptive*, in that they are based on clusters that are derived from an ensemble of samples, as opposed to being crafted for a particular landscape. See Appendix F.

As for the required gradients, these are generally harder to estimate. Nevertheless, for the particular gradient $\nabla h_{G,\tilde{G}^c}$, the problem is substantially mitigated by noting that we are only interested in its evaluation on ∂G and $\partial\tilde{G}$, each of which is a level set of $h_{G,\tilde{G}^c}$

($h_{G,\tilde{G}^c} = 1$ on G and 0 on $\tilde{G}$). Consequently, on each surface the gradient is in the normal direction and we need only estimate its magnitude. And for this purpose it is enough to know the values of $h_{G,\tilde{G}^c}$ on a surface close to G and interior to $\tilde{G}\backslash G$ (for estimating $\nabla h_{G,\tilde{G}^c}$ on G) and on another surface close to $\tilde{G}$ and also interior to $\tilde{G}\backslash G$ (for estimating $\nabla h_{G,\tilde{G}^c}$ on $\tilde{G}$). Two such surfaces would be ∂S_1 and ∂S_{n-1}, were we to apply the shell method with $R = G$ and $\tilde{R} = \tilde{G}$, since, as already noted, a byproduct of the method is an estimate of $h_{R,\tilde{R}^c}$ on all of the shells. Alternatively, in the interest of better accuracy, the method could be run twice, once with $S = S_1$, a well-chosen outer approximation of G, and then again with $S = S_{n-1}$, a well-chosen inner approximation of $\tilde{G}$.

V.   Numerical Experiments[1]

To verify our theoretical results and validate the capacity-estimation algorithm, we carry out numerical experiments with the following idealization: the configuration space, Ω, is the unit ball in $\mathbb{R}^n$ ($\Omega = \mathcal{B}(0,1)$, where $\mathcal{B}(x,r) \triangleq \{y : ||y-x|| < r\}$). The configuration itself, $X = X_t$, is confined to Ω by a reflecting boundary at $\partial\Omega$, and within Ω the dynamics are assumed to be well approximated by the first-order (high-viscosity) Langevin equation,

$$\mathrm{d}X_t = -\nabla U(X_t)\mathrm{d}t + \mathrm{d}W_t \tag{9}$$

where W_t is an n-dimensional Brownian motion and U is a potential energy. There are only two targets,

$$A \triangleq \mathcal{B}(x_A, r_A)$$
$$B \triangleq \mathcal{B}(x_B, r_B)$$

which can be completely or just partially contained in Ω (note that in the case where the targets are only partially contained in Ω, we recover the narrow escape problem). Given an initial condition $X_0 \in \Omega\backslash(A \cup B)$, we are interested to know whether the dynamics carry the system into A or B first, in the special case that U is smooth beyond the immediate neighborhoods of A and B. To this end, introduce neighborhoods $\dot{A} = \mathcal{B}(x_A, r_{\dot{A}})$ and

$\tilde{A} = \mathcal{B}(x_A, r_{\tilde{A}})$ such that $r_A < r_{\dot{A}} < r_{\tilde{A}}$, and $\dot{B} = \mathcal{B}(x_B, r_{\dot{B}})$ and $\tilde{B} = \mathcal{B}(x_B, r_{\tilde{B}})$ such that $r_B < r_{\dot{B}} < r_{\tilde{B}}$, and assume, in the extreme case, that $\nabla U(x) = 0$ for all $x \in \Omega \backslash (\dot{A} \cup \dot{B})$. If we let $h_{A,B}(x)$ be the probability that X_t reaches A before reaching B ("first-passage at A"), which depends on the starting configuration $X_0 = x$, then more specifically we are interested in computing approximations to $h_{A,B}(x)$ using only the behavior of U in the vicinity of the targets, provided that x, the starting configuration, is sufficiently far from $A \cup B$. The set M is idealized by assuming that $\nabla U(x) = 0$ outside of $\dot{A} = \mathcal{B}(x_{\dot{A}}, r_{\dot{A}})$ and $\dot{B} = \mathcal{B}(x_{\dot{B}}, r_{\dot{B}})$ and "sufficiently far away" means outside of $\tilde{A} \cup \tilde{B}$, where $\tilde{A} = \mathcal{B}(x_{\tilde{A}}, r_{\tilde{A}})$ and $\tilde{B} = \mathcal{B}(x_{\tilde{B}}, r_{\tilde{B}})$.

We experimented with this two-target system in $n = 5$ dimensions. Our experiments test the overall approximation to $h_{A,B}$ developed in §III-IV as well as each of the three components, separately: ϵ-flatness, the role of capacities, and the methodology developed for estimating capacities. The experimental setup is sufficiently simple to allow exhaustive simulation for approximating ground truth. In each experiment, we compare the results of using the approximations developed here to the results from an ensemble of first-passage events simulated by simply running the diffusion 2,000 times at each of 100 randomly chosen points in $\Omega \backslash (\tilde{A}, \tilde{B})$. There are two sets of experiments: In the first (a kind of "sanity check"), the targets A and B are completely in Ω, and the potential U is flat everywhere outside of the targets A and B (i.e. the diffusion is Brownian motion). In the second, the targets A and B are only partially contained in Ω, resulting in a narrow-escape type problem, and there are complex landscapes in the vicinities of the targets, i.e. within $\dot{A}$ and $\dot{B}$.

If the targets A and B are both small (in the sense that $r_A, r_B \ll 1$), and the starting configuration $x \in \Omega \backslash (\tilde{A}, \tilde{B})$ is sufficiently far from $A \cup B$, then Theorems 2 and 1 are both in force, and hence the first-passage probability $h_{A,B}(x)$, on $\Omega \backslash (\tilde{A}, \tilde{B})$, is approximately a constant, and the value depends only on the two local capacities $\text{cap}(A, \tilde{A})$ and $\text{cap}(B, \tilde{B})$:

$$h_{A,B}(x) \approx \frac{\text{cap}(A, \tilde{A})}{\text{cap}(A, \tilde{A}) + \text{cap}(B, \tilde{B})}$$

We need to compute, or approximate, $\text{cap}(A, \tilde{A})$ and $\text{cap}(B, \tilde{B})$. We will work through the details for $\text{cap}(A, \tilde{A})$, but the identical considerations apply to $\text{cap}(B, \tilde{B})$. We start with the flux representation established in the Proposition, and the numerical approximation from Equation (8), which reduces the problem to selecting G and $\tilde{G}$ and then applying the shell method, as described in §IV. In the current setup, good choices for G and $\tilde{G}$ are $G = \dot{A}$ and

$\tilde{G} = \tilde{A}$, as can be seen from the following observations:

1. Recall that $h_{A,\tilde{A}^c}(x)$ is the probability of first exiting $\tilde{A}\backslash A$ at ∂A rather than at $\partial\tilde{A}$, given that the process started at x. Consequently $h_{A,\tilde{A}^c}(x) = 0$ for all $x \in \partial\tilde{A}$, and hence also on $\partial\tilde{G}$. Hence, with reference to Equation (8), we need only consider the flux approximation on ∂G:

$$\text{cap}(A, \tilde{A}) \approx -|\partial G| \frac{\sum_{i=1}^{m} h_{A,\tilde{A}^c}(y_i)\mathfrak{n}(y_i) \cdot \nabla h_{G,\tilde{G}^c}(y_i)}{\sum_{i=1}^{m} e^{U(y_i)}} \tag{10}$$

where $y_1, \ldots, y_m$ are independent samples from $\mathscr{P}(dx) = \frac{1}{Z}e^{-U}\mathscr{H}(dx)$ on ∂G, $\mathfrak{n}(x)$ faces outward from G, and compared to (8), we have used the fact that in the current setup $a(x)$ is the identity I.

2. The surface area $|\partial G|$ is just the area of the 4-sphere (in five dimensions), with radius $r_{\dot{A}}$:

$$|\partial G| = \frac{2\pi^{\frac{5}{2}}}{\Gamma(\frac{5}{2})}r_{\dot{A}}^4$$

3. Furthermore, since $\nabla U(x) = 0$ on $\Omega\backslash(\dot{A} \cup \dot{B})$ and the diffusion is unchanged by a constant shift of the potential, we can assume that $U(x) = 0$ on $\Omega\backslash(\dot{A} \cup \dot{B})$. Since $G = \dot{A}$ and since U is continuous, $U(x) = 0$ for all $x \in \partial G$. Hence $\sum_{i=1}^{m} e^{U(y_i)} = m$.

4. Since U is flat on $\tilde{G}\backslash G$, the first-passage function $h_{G,\tilde{G}^c}$ is that of a standard Brownian motion between two concentric spheres. The PDE in Equation (A1) of Appendix A reduces to an instance of Laplace's equation, with analytic solution[33]

$$h_{G,\tilde{G}^c}(x) = \frac{1}{r_{\dot{A}}^{-3} - r_{\tilde{A}}^{-3}}\|x - x_A\|^{-3} - \frac{r_{\tilde{A}}^{-3}}{r_{\dot{A}}^{-3} - r_{\tilde{A}}^{-3}}$$

from which the gradient is found to be

$$\nabla h_{G,\tilde{G}^c}(x) = \frac{-3}{r_{\dot{A}}^{-3} - r_{\tilde{A}}^{-3}}\|x - x_A\|^{-4}\frac{x - x_A}{\|x - x_A\|} = \frac{-3}{r_{\dot{A}}^{-3} - r_{\tilde{A}}^{-3}}\|x - x_A\|^{-4}\frac{x - x_A}{\|x - x_A\|}$$

And since $\|x - x_A\| = r_{\dot{A}}$ and $\frac{x - x_A}{\|x - x_A\|} = \mathfrak{n}(x)$,

$$\mathfrak{n}(x) \cdot \nabla h_{G,\tilde{G}^c}(x) = \frac{-3}{r_{\dot{A}}^4(r_{\dot{A}}^{-3} - r_{\tilde{A}}^{-3})}$$

5. It remains to choose a sample $y_1, \ldots, y_m$ from $\mathscr{P}(dx)$ on G, and estimates of the accompanying values of $h_{A,\tilde{A}^c}(y_i)$, $i = 1, \ldots, m$. Here, the shell method (Appendix F) can be used, with $R = A$, $\tilde{R} = \tilde{A}$, and $S = G$, resulting in the desired samples $y_1, \ldots, y_m$ and estimates of $h_{A,\tilde{A}^c}(y_1), \ldots, h_{A,\tilde{A}^c}(y_m)$, say $u_1, \ldots, u_m$.

Putting together the pieces, the approximation in (10) becomes

$$\text{cap}(A, \tilde{A}) \approx \frac{6\pi^{\frac{5}{2}}}{\Gamma(\frac{5}{2})(r_{\tilde{A}}^{-3} - r_{\tilde{A}}^{-3})} \frac{1}{m} \sum_{i=1}^{m} u_i \tag{11}$$

The approximation we used for $\text{cap}(B, \tilde{B})$ is the same, but with the substitutions $A \to B$ and $\tilde{A} \to \tilde{B}$.

A. Brownian Diffusion

The first set of experiments test the approach in the simplest possible case: there is no gradient in U anywhere outside of the targets. Even though the resulting diffusion is just a standard Brownian motion, there are few symmetries in the configuration space and hence still no closed-form solution for the first-passage probabilities.

In this set of experiments, we fixed the target centers $x_A = (0.5, 0.6, 0.0, 0, 0, 0.0)$, $x_B = (-0.7, 0.0, 0.0, 0, 0, 0.0)$ and the radiuses $r_{\tilde{A}} = r_{\tilde{B}} = 0.2$, and tested the overall approximation in three different cases, with targets of three different sizes: small (where $r_A = 0.02, r_B = 0.04$), medium (where $r_A = 0.05, r_B = 0.075$) and large (where $r_A = r_B = 0.15$). An illustration of the three different cases and the corresponding results are shown in Figure 2.

1. Are first-passage probabilities approximately constant outside of $\tilde{A} \cup \tilde{B}$?

Is it true that in regions with golf-course potentials, the hitting probability is approximately constant over initial conditions that are modestly far away from the targets? In other words, is $h_{A,B}$ ε-flat on $\Omega \backslash (\tilde{A} \cup \tilde{B})$? Theorem 2 shows that this must hold in the limiting regime of small r_A, r_B or large n, but it is not obvious how small r_A, r_B need to be in order for the model to be operating within this regime.

In each of the three different cases, we ran 2,000 diffusion simulations at each of 100 randomly selected initial conditions in the region $\mathcal{B}(0,1) \backslash (\tilde{A} \cup \tilde{B})$, yielding 100 well-estimated probabilities of hitting A before B. The histograms of these probabilities can be be found in Figure 2. As we can see, as the targets become smaller, the observations fall in narrower windows, and the empirical distribution becomes more peaked. Note that in all three cases,
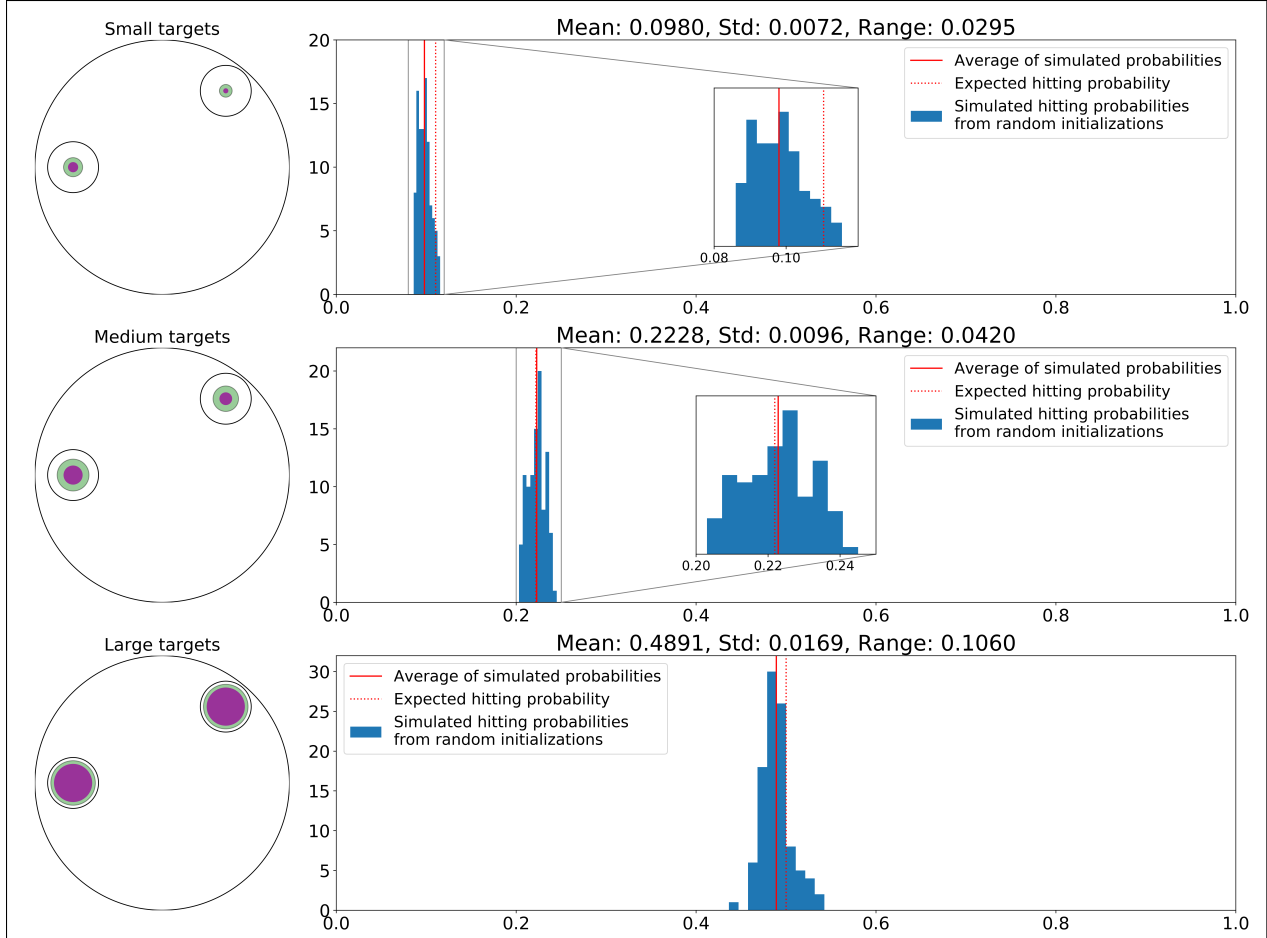
Figure 2. **First-passage probabilities: direct simulations vs. evaluation of local capacities.** Local capacities can accurately answer the question "where will we go next?" We start by designating two targets, A and B. For any given initial condition, the task is to determine the probability that the diffusion will hit A first. We study this question in the context of the simplest possible case, where we have a flat energy landscape and the diffusion is simply a Brownian motion, and consider 100 random initial locations which are modestly far away from either target. We consider three different cases (small, medium and large targets), as illustrated in the left quater of the figure. For each initial location, we conduct 2000 simulations to estimate the probability of hitting target A first. We see that the hitting probability is approximately constant for initial conditions which are modestly far away from the targets when the targets are small. Furthermore, the value of this constant is very nearly proportional to the ratio of the local capacities. In summary, in cases where the targets are small, first-passage probabilities are accurately estimated using only local simulations around the targets, and do not require any computations that involve the large space around A and B.

we can say h is ε-flat, with ε being approximately 0.0295 for small targets, 0.0420 for medium targets, and 0.1060 for large targets. However, being ε-flat with a small ε is more interesting than with a large one, as, according to Theorem 1, a smaller ε gives us a tighter error bound

for our overall approximation to the first-passage probability.

2. Are first-passage probabilities proportional to capacity?

According to Theorem 1, in light of the ε-flatness of $h_{A,B}$ with respect to $\Omega\backslash(\tilde{A}\cup\tilde{B})$, $h_{A,B}(x)$ should be well approximated by

$$p_A \doteq \frac{\mathrm{cap}(A,\tilde{A})}{\mathrm{cap}(A,\tilde{A}) + \mathrm{cap}(B,\tilde{B})} \tag{12}$$

for $x \in \mathcal{B}(0,1) \setminus (\tilde{A}\cup\tilde{B})$. In the current experiment, with $\nabla U = 0$ on $\tilde{A}\backslash A$ and $\tilde{B}\backslash B$, the capacities can be computed analytically, e.g. from Corollary 1, with $S = A$ and $S = B$:

$$\mathrm{cap}(A,\tilde{A}) = \frac{6\pi^{\frac{5}{2}}}{\Gamma(\frac{5}{2})(r_A^{-3} - r_{\tilde{A}}^{-3})} \qquad \mathrm{cap}(B,\tilde{B}) = \frac{6\pi^{\frac{5}{2}}}{\Gamma(\frac{5}{2})(r_B^{-3} - r_{\tilde{B}}^{-3})} \tag{13}$$

and hence

$$p_A = \frac{\frac{1}{r_A^{-3} - r_{\tilde{A}}^{-3}}}{\frac{1}{r_A^{-3} - r_{\tilde{A}}^{-3}} + \frac{1}{r_B^{-3} - r_{\tilde{B}}^{-3}}}$$

For the three different cases we used in our experiments, $p_A \approx 0.1104$ for small targets, $p_A \approx 0.2219$ for medium targets, and $p_A = 0.5$ for large targets. In all cases, this probability is close to the average found by direct simulations.

3. Accuracy of the shell method.

Lastly, we check the accuracy of the capacity estimation algorithm that we call the shell method. Here, the exact values are available from the formulas in (13), while the approximate values come from two applications of (11). For small targets, the true capacities are $\mathrm{cap}(A,\tilde{A}) = 0.000632$ and $\mathrm{cap}(B,\tilde{B}) = 0.005094$, while shell method estimates them to be 0.000549 and 0.004699, respectively. For medium targets, the true capacities are $\mathrm{cap}(A,\tilde{A}) = 0.01002626$ and $\mathrm{cap}(B,\tilde{B}) = 0.03516428$, while shell method estimates them to be 0.00930769 and 0.03362453, respectively. For large targets, the true capacities are $\mathrm{cap}(A,\tilde{A}) = \mathrm{cap}(B,\tilde{B}) = 0.4609372$, while shell method estimates them to be 0.45244093 and 0.45153703, respectively. [3]

Had we used the estimated capacities instead of the actual capacities for computing p_A from Equation (12) the approximation of the first-passage probability, given $x \in \mathcal{B}(0,1) \setminus$

---

[3] With reference to Appendix F, the following parameters were used to implement the shell method: $m = 2, n = 4, N_p = 100, N_b = 3, N_s = 1000$, and a time-step of 10^{-7}.
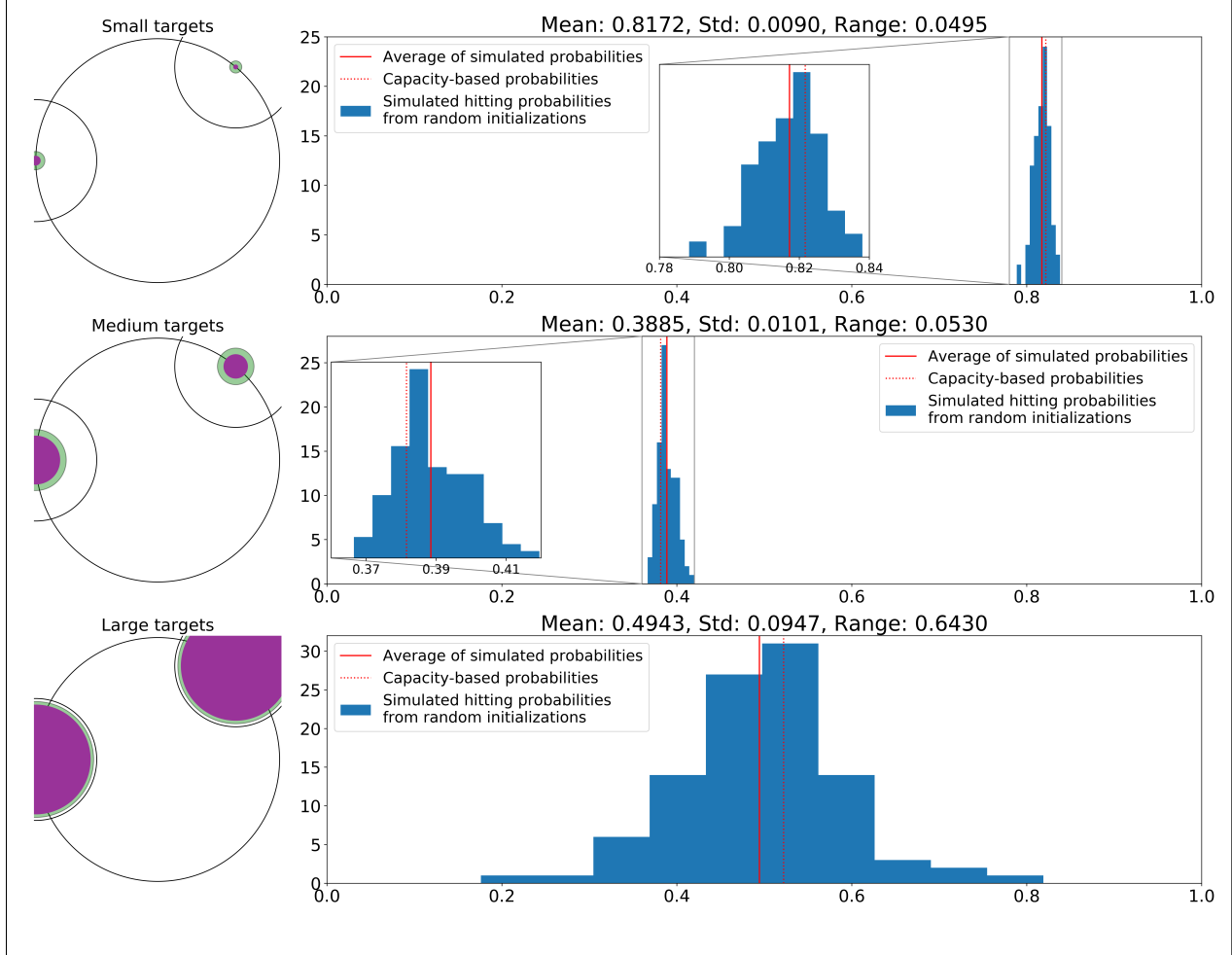
Figure 3. **First-passage probabilities direct simulations vs. evaluation of local capacities.** The setup is similar to Figure 2, with the only differences being that the targets A and B are only partially contained in Ω, and the energy landscape becomes complicated near the targets. We again consider three different cases (small, medium and large targets), as illustrated in the left quater of the figure. For each initial location, we conduct 2000 simulations to estimate the probability of hitting target A first. While the first-passage probabilities vary significantly in the case of large targets, they are approximately constant in the case of small and medium targets, for initial conditions which are modestly far away from the targets. Furthermore, the value of this constant is very nearly proportional to the ratio of the local capacities. In summary, in these simulations first-passage probabilities are accurately estimated using only local simulations around the targets, and do not require any computations that involve the large space around A and B.

$(\tilde{A} \cup \tilde{B})$, would have been 0.1091 instead of 0.1104 for small targets, 0.2168 instead of 0.2219 for medium targets, and 0.5005 instead of 0.5 for large targets.

In summary, all three components of the approach performed well in the Brownian motion test case.

B. Nontrivial Landscape

We performed the same tests, but with the targets A and B only partially contained in Ω (resulting in a narrow-escape type problem), and a complex energy landscape in the neighborhoods of the targets, i.e. on $\dot{A}\backslash A$ and $\dot{B}\backslash B$. More concretely, we fixed the target centers $x_A = (0.6402, 0.7682, 0.0, 0, 0, 0.0)$, $x_B = (-1.0, 0.0, 0.0, 0, 0, 0.0)$ and the radiuses $r_{\tilde{A}} = r_{\tilde{B}} = 0.5$, and tested the overall approximation in three different cases, with targets of three different sizes: small (where $r_A = 0.02, r_{\dot{A}} = 0.05, r_B = 0.04, r_{\dot{B}} = 0.075$), medium (where $r_A = 0.1, r_{\dot{A}} = 0.15, r_B = 0.2, r_{\dot{B}} = 0.25$) and large (where $r_A = r_B = 0.45, r_{\dot{A}} = r_{\dot{B}} = 0.475$). More details of the specification can be found in Appendix G. An illustration of the three different cases and the corresponding results are shown in Figure 3.

1. Are first-passage probabilities approximately constant outside of $\tilde{\boldsymbol{A}} \cup \tilde{\boldsymbol{B}}$?

Following the same procedure used in §V A 1 we tested for the near-constancy of $h_{A,B}$ on $\Omega\backslash(\tilde{A} \cup \tilde{B})$. The histograms of the probabilities are illustrated in Figure 3. As we can see, for the large targets case, the first-passage probabilities are fairly spread-out, but as the targets become smaller, they become significantly more concentrated. For both the small and medium targets case, h is ε-flat, with ε being approximately 0.0495 and 0.0530, respectively.

2. Are first-passage probabilities proportional to capacity?

In the previous experiments we were able to compute the capacities in closed form, and use p_A, from Equation (12), to directly verify the conclusion of Theorem 1. This is not possible in the current experiments. We are forced instead to use the estimated capacities. For small targets, we obtained the estimate $p_A \approx 0.8216$, which is within 0.5% of 0.8172, the average found by direct simulations. For medium targets, we obtained the estimate $p_A \approx 0.3815$, which is within 2% of 0.3885, the average found by direct simulations.[4]

Notable in the results for the small targets is the fact that the larger target, B, is substantially less likely than A to be visited first. Evidently, the energy in $\dot{B}\backslash B$, the region surrounding B, introduces a significant barrier to the diffusion process, at least in comparison to the energy surrounding A. Keep in mind that the process here is identical to the one in the previous experiments, i.e. Brownian motion, for so long as the process remains outside of $\dot{A} \cup \dot{B}$, and that in those experiments the first-passage occurred at B approxi-

---

[4]Using the following parameters (Appendix F): $m = 2$, $N_p = 3000$, $N_b = 5$, $N_s = 1000$, with time-step 10^{-6}. For target A we used $n = 4$ and for the larger target B we used $n = 5$.

mately ten times more often than at A. Evidently, the process is much more likely to exit $\dot{B}\backslash B$ at $\partial\dot{B}$ than at ∂B, at least in comparison to the dynamics in $\dot{A}\backslash A$. These observations serve to further illustrate the role of local capacities and the importance of their accurate approximation.

3. Accuracy of the shell method.

As already remarked, the nontrivial energy landscape precludes a direct assessment of the accuracy of the capacity estimation algorithm. It is not possible to obtain exact values for the capacity. Therefore, we cannot directly test whether our algorithm is accurately estimating the capacities. However, the good agreement between the estimated value of p_A and the results of straightforward simulation constitute indirect evidence supporting the approximations, and the accuracy of the shell method in particular.

Concerning computational efficiency, it is difficult to make a direct comparison between the capacity-estimation approach and straightforward simulation. There are many parameters and, besides, run times will depend on the dimension and details of the energies, possibly affecting the two approaches differently. In our experiments, for direct simulations we used the "walk-on-spheres" method to simulate trajectories in the flat region,[34] JIT compilation to remove loop overhead, multi-CPU parallelization, and the coarsest time step that yielded accurate results. As for capacity estimation, we made no effort to adjust the number of samples or the discretization parameters. Under these conditions, a single run of the direct simulation took about as long as estimating the two capacities.

Assume that $h_{A,B}(x)$ is ε-flat relative to $\Omega\backslash(\tilde{A}\cup\tilde{B})$. Both methods suffer if ε is large: direct simulation because it will depend on the initial condition, which is unknowable in any realistic experiment, and capacity estimation because the capacity ratio has a built-in error (Theorem 1) that depends on ε. If we assume that ε is negligible, then for a fixed $x \in \Omega\backslash(\tilde{A}\cup\tilde{B})$ we can more-or-less directly compare the standard deviations of the capacity-based estimation of $p \doteq h_{A,B}(x)$ via the shell method to direct simulation via repeated-samples. For example, under the specific (albeit idealized) circumstances of the experiments for small targets in §V A, about how many direct-simulation samples would be needed to attain a confidence interval for p of comparable width as from a single sample using capacity estimation by the shell method? The binomial estimator from n direct samples has standard deviation $\sqrt{\frac{p(1-p)}{n}}$, which we can compare to the empirical standard deviation, $\hat{\sigma} \approx 0.006$,

from 100 runs of the shell method estimating p. Recall from §V A that $p \approx 0.1100$, in which case approximately $n = 2,700$ runs of direct simulation would be needed to get a comparable confidence interval. Bear in mind that a single run of the shell method requires about as much time as a single run of direct diffusion. It would appear, then, that capacity-based estimation of first-passage probabilities can be several orders-of-magnitude faster than direct simulation.

VI. Discussion

This paper arises from an elementary observation: if the hitting probability is nearly the same for every initial condition in a region M, then it is reasonable to approximate that that it is exactly the same for every initial condition in M. Applying this approximation to the appropriate variational problem, we find that the hitting probability is well-approximated in terms of integrals computed away from M; we dub these integrals the "first-passage capacities." These capacities can be approximately computed using a milestoning-like technique, as described in §IV.

This begs the question: is it ever true that hitting probabilities are nearly the same for every initial condition in large region, M? Theorem 2 shows that the answer is yes. Indeed, the answer is yes whenever the mixing rate of the diffusion is fast relative to the typical escape time from M. In practice, this condition may not always be easy to check.

A major outstanding limitation of this work is that we provide no strategy for checking the ε-flatness condition. In theory, bounds on the Lipschitz constant of the energy function and the Poincare constant for M should be sufficient to ensure this condition, but we leave this for future work. For now, we content ourselves that the condition certainly holds when the ambient dimension is at least three and the targets become small. Moreover, when the dimension is very large then even targets with modestly large diameter can have very small overall volume, yielding a similar result.

The second major limitation of this work is that first-passage capacities do not directly inform us about the overall timescale on which the diffusion is operating. The mean first-passage capacities are often inversely proportional to the first-passage times, but the overall proportionality constant is lost in this analysis. In some limited cases, methods from the narrow escape literature may enable us to determine this overall constant.

In general, it may turn out that estimating first-passage times is profoundly more difficult than estimating first-passage hitting probabilities. In this work we showed that the first-passage probabilities are sometimes invariant to the diffusion dynamics on the interior of a large set M, but the first-passing timing admit no such invariance. If the dynamics inside of M are genuinely intricate, it appears that estimating hitting times will always require a correspondingly intricate analysis.

We conclude by considering a possible future direction for this work. Let us consider the case where we have many targets, $A_1, A_2 \cdots A_n$, and the path between any two of the targets must pass through a set M. In this case, assuming the ε-flatness condition holds on M, the order in which the process explores the targets could be accurately modeled using first-passage capacities alone. In future we hope to explore this possibility.

APPENDIX

A.   Three Perspectives on Hitting Probabilities

Many of our results are based on the fact that hitting probabilities can actually be seen from three distinct perspectives. To prepare for these results, we take a moment to review these three perspectives here. Let $A, B \subset \Omega$, disjoint, open with smooth boundary.

1. Hitting probabilities. Let $\tau_S \triangleq \inf\{t : X_t \in S\}$ for any set S and $h_{A,B}(x) \triangleq \mathbb{P}(X_{\tau_{A \cup B}} \in \partial A | X_0 = x)$.

2. Elliptic equation. Let $h_{A,B}^{\mathrm{dir}}(x)$ denote the solution to the partial differential equation:

$$0 = \sum_{i=1}^{n} b_i(x) \frac{\partial u(x)}{\partial x_i} + \frac{1}{2} \sum_{i=1}^{n} \sum_{j=1}^{n} a_{ij}(x) \frac{\partial^2 u(x)}{\partial x_i \partial x_j} \quad x \notin \bar{A}, \bar{B} \tag{A1}$$

$$1 = u(x), x \in A$$

$$0 = u(x), x \in B$$

$$0 = \mathfrak{n}(x)^T a(x) \nabla u(x), x \in \partial \Omega$$

   This solution is unique and smooth.[35] What's more, it is equal to the hitting probability function: $h_{A,B}^{\mathrm{dir}}(x) = h_{A,B}(x)$ (cf. Section 6.7 of Chen[36]).

3. Variational form. For any open set $S \subset \Omega$ let $\mathscr{E}_S(f,g) \triangleq \int_S \nabla f(x)^T a(x) \nabla g(x) \rho(dx)$ denote the "Dirichlet Form" of f, g on the domain S. Let $\mathscr{L}^2(S, \rho)$ denote the Hilbert space of functions on S which are square-integrable with respect to ρ. Let $\mathcal{H}^1(S, \rho) = W^{1,2}(S) \subset \mathscr{L}^2(S)$ denote the corresponding once-weakly-differentiable Hilbert Sobolev space. We define $h_{A,B}^{\mathrm{var}}(x)$ as the solution to

$$\min_{u \in \mathcal{H}^1(S)} \quad \mathscr{E}_S(u, u)$$

$$\text{subject to} \quad u(x) = 1, x \in \partial A$$

$$u(x) = 0, x \in \partial B$$

   where $S = \Omega \backslash (A \cup B)$. This solution is unique and equal to $h_{A,B}^{\mathrm{dir}}$ on S (cf. Section

4 of Dret[37]). This variational perspective leads us to the notion of the "condenser capacity" associated with $h_{A,B}$. It is defined as

$$\mathrm{cap}(A, \Omega\backslash B) \triangleq \mathscr{E}_S(h_{A,B}, h_{A,B})$$

where again $S = \Omega\backslash(A \cup B) = (\Omega\backslash B)\backslash A$.

We will use all three of these perspectives to show our results. For example, consider how the hitting probability perspective helps us show a result about capacities:

Proposition 2. *Let* $A \subset \tilde{A}, B \subset \tilde{B}$ *with* $\tilde{A}, \tilde{B}$ *disjoint. Then*

$$\mathrm{cap}(A \cup B, \tilde{A} \cup \tilde{B}) = \mathrm{cap}(A, \tilde{A}) + \mathrm{cap}(B, \tilde{B})$$

Proof. This result is certainly known, but we include a proof here because we were unable to find a proof in the literature. Since $\tilde{A}, \tilde{B}$ are disjoint and X is continuous, the process cannot cross from one to the other without hitting the boundary. Thus we have $\tau_{\partial\tilde{A}\cup\partial\tilde{B}\cup\partial A\cup\partial B} = \tau_{\partial\tilde{A}\cup\partial A}$ as long as $X_0 \in \tilde{A}$. We get a symmetric result if $X_0 \in \tilde{B}$. It follows that

$$h_{A\cup B, (\tilde{A}\cup\tilde{B})^c}(x) = \begin{cases} h_{A,\tilde{A}^c}(x) & \text{if } x \in \tilde{A} \\ h_{B,\tilde{B}^c}(x) & \text{if } x \in \tilde{B} \end{cases}$$

We can now use this probabilistic perspective to help us understand the capacity by articulating it as the Dirichlet form on the relevant hitting probability functions

$$
\begin{aligned}
\mathrm{cap}(A \cup B, \tilde{A} \cup \tilde{B}) &= \int_{\tilde{A}\cup\tilde{B}\backslash(A\cup B)} \|\sigma\nabla h_{A\cup B, (\tilde{A}\cup\tilde{B})^c}\|^2 \rho(dx) \\
&= \int_{\tilde{A}\backslash A} \|\sigma\nabla h_{A,\tilde{A}^c}\|^2 \rho(dx) + \int_{\tilde{B}\backslash B} \|\sigma\nabla h_{B,\tilde{B}^c}\|^2 \rho(dx) \\
&= \mathrm{cap}(A, \tilde{A}) + \mathrm{cap}(B, \tilde{B})
\end{aligned}
$$

as desired. □

B. Proof of Theorem 2

Theorem 2. *(Examples of ε-flatness). Let $\mathcal{B}(x,r) = \{y : \|x - y\| < r\}$ denote the ball of radius r centered at x. Recall that the process X behaves according to the stochastic differential equation $dX_t = b(X_t)dt + \omega(X_t)dW_t$ contrained to lie inside a set Ω by normally reflecting boundaries.*

1. *Let $\Omega \in \mathbb{R}^n, n \geq 3$ be convex and open with diameter less than or equal to 1. Fix any points $x_A, x_B \in \mathbb{R}^n$. For any $r, \varepsilon > 0$ we can find $r' > 0$ such that $h_{A,B}$ is ε-flat on $\Omega \backslash \mathcal{B}(x_A, r) \cup \mathcal{B}(x_B, r)$ for any $A \subset \mathcal{B}(x_A, r'), B \subset \mathcal{B}(x_A, r')$ as long as $b(x) = 0, \Omega(x) = I$ for $x \in \Omega \backslash \mathcal{B}(x_A, r') \cup \mathcal{B}(x_B, r')$.*

2. *Fix $r, \varepsilon > 0$ and also fix $r' < r$. We can then find n with the following property. For any convex open set $\Omega \in \mathbb{R}^n$ with diameter less than or equal to 1, any x_A, x_B such that $\mathcal{B}(x_A, r), \mathcal{B}(x_B, r) \subset \Omega$, and any $A \subset \mathcal{B}(x_A, r'), B \subset \mathcal{B}(x_B, r')$, we have that $h_{A,B}$ is ε-flat on $\Omega \backslash \mathcal{B}(x_A, r) \cup \mathcal{B}(x_B, r)$ as long as $b(x) = 0, \Omega(x) = I$ for $x \in \Omega \backslash \mathcal{B}(x_A, r') \cup \mathcal{B}(x_B, r')$.*

Proof. Let $\dot{A} = \mathcal{B}(x_A, r'), \dot{B} = \mathcal{B}(x_B, r')$. Let $\{Z_t\}_t$ denote a Brownian motion trapped inside Ω and coupled to X such that $X_t = Z_t$ for all $t \leq \tau = \left\{\inf t : X_t \in \dot{A} \cup \dot{B}\right\}$ (we can do this because we assumed that X behaves like Brownian motion outside of $\dot{A}, \dot{B}$). Let Z_∞ denote the stationary distribution of Z, i.e. the uniform distribution on Ω. Using Lemma 1, we have that

$$|\mathbb{E}\left[h_{A,B}(Z_t) - h_{A,B}(Z_\infty)|Z_0 = x\right]| \leq \frac{1}{t} \qquad \forall x$$

On the other hand, Dynkin's formula gives that

$$h_{A,B}(x) = \mathbb{E}\left[h_{A,B}(Z_{\tau \wedge t})|Z_0 = x\right] \qquad \forall t, x$$

Putting those two facts together:

$$|h_{A,B}(x) - \mathbb{E}\left[h_{A,B}(Z_\infty)\right]|$$

$$= |\mathbb{E}\left[h_{A,B}(Z_{\tau \wedge t}) - h_{A,B}(Z_\infty)|Z_0 = x\right]|$$

$$\leq |\mathbb{E}\left[h_{A,B}(Z_{\tau \wedge t}) - h_{A,B}(Z_t)|Z_0 = x\right]| + |\mathbb{E}\left[h_{A,B}(Z_t) - h_{A,B}(Z_\infty)|Z_0 = x\right]|$$

$$\leq \mathbb{P}\left(\tau \leq t|Z_0 = x\right) + \frac{1}{t}$$

To make this small, it thus suffices to get t large but keep $\mathbb{P}\left(\tau \leq t\right)$ small. In short, it suffices to show that τ is usually big. We prove this differently in the two different cases:

1. The first example follows because the targets are vanishing into nothing, so it is no surprise that the time to hit the targets will get longer and longer. However, note that this intuition is valid only because the ambient dimension n is at least three (which we have assumed throughout). A formal proof of this argument can be found in Lemma 2.

2. The second example is similar; even though the targets maintain the same diameter, their relative volume is vanishing because the ambient dimension n is increasing. Thus the targets are effectively becoming smaller, so the hitting time increases. This matter is a bit trickier, and so for this second case note we have made additional requirements that $\mathcal{B}\left(x_A, r\right), \mathcal{B}\left(x_B, r\right) \subset \Omega$. A formal proof of this argument can be found in Lemma 3.

$$\square$$

Lemma 1. *(Uniform ergodicity) Let $\Omega \subset \mathbb{R}^d$ be a convex set with diameter ξ and let M denote a Brownian motion trapped by reflecting boundaries inside Ω. The distribution of M_t converges uniformly to the uniform distribution, in the sense that:*

$$\sup_{f: \; \Omega \to [0,1]} |\mathbb{E}[f(M_t) - f(Z)|M_0 = x]| \leq \xi^2/4t \qquad \forall x \in \Omega, t > 0$$

where Z is uniformly distributed on Ω.

Proof. Per Loper [38],

$$\sup_{f:\ \Omega \to [0,1]} |\mathbb{E}[f(M_t) - f(Z)|M_0 = x]| \le \mathbb{P}(\tau > 4t)$$

where τ is the first exit time of a one-dimensional Brownian motion from the interval $[-\xi, \xi]$ when initialized at the origin. Dynkin's formula gives that $\mathbb{E}[\tau] = \xi^2$. Hence, by the Markov inequality, $\mathbb{P}(\tau > 4t) \le \xi^2/4t$. $\qquad\square$

Lemma 2. *Let Z denote a Brownian motion trapped inside a convex bounded open set $\Omega \subset \mathbb{R}^n$ with smooth boundary. We further assume that $n \ge 3$. Fix $x \in \mathbb{R}^n$ and $r, \epsilon > 0$. Let τ_A denote $\inf\{t : \ Z_t \in A\}$ for any set A. We can always find $r_1 > 0$ such that $\mathbb{P}(\tau_A < 1/\epsilon | Z_0 = z) < \epsilon$ for all $z \notin \mathcal{B}(x, r_3)$ and all $A \subset \mathcal{B}(x, r_1)$.*

Proof. First consider the case that $x \in \Omega$. To measure the time it takes to hit $\mathcal{B}(x, r_1)$, we will make use of two additional concentric spheres around x. First, find r_3 such that $\mathcal{B}(x, r_3) \subset \Omega$. Second, let $r_2 = \sqrt{r_1 r_3}$, an intermediate radius. We will use these spheres to break the trajectory of Z into smaller manageable pieces. If $\|Z_0 - x\| > r_3$, the first part of the trajectory must carry it to a radius of r_2 before it reaches r_1. The next part of the trajectory will then do one of two things: either it will carry on to r_1 or it will first exit the ball of radius r_3. Assuming it exits the ball of radius r_3, the strong Markov property can be used to show that we are essentially in the same place we started. Under this latter condition, the total time will be the the time we've spent so far plus a new variable which has the same properties as the original time. We can use this recursive relation to put a lower bound on the overall time.

Let us make this rigorous. To measure the tails of τ, we will be interested in

$$g(z) = \mathbb{E}\left[e^{-\frac{1}{2}\tau}|Z_0 = z\right]$$

To get a lower bound on the moments of τ, we need to get an upper bound on this object. To do so, we will use two objects of interest:

$$g_3 = \sup_{z:\ \|z - x\| = r_3} g(z)$$

$$g_2 = \sup_{z:\ \|z - x\| = r_2} g(z)$$

using two stopping times of interest:

$$T_2 = \inf\{t : \ \|Z_t - x\| = r_2\}$$

$$T_3 = \inf\{t > T_1 : \ \|Z_t - x\| = r_3\}$$

Applying the strong Markov property, we observe that

$$g_2 = \sup_{z: \ \|z-x\|=r_2} \mathbb{E}\left[\mathbb{E}\left[e^{-\frac{1}{2}\tau}|Z_{T_3 \wedge \tau}\right]|Z_0 = z\right]$$

$$= \sup_{z: \ \|z-x\|=r_2} \mathbb{E}\left[e^{-\frac{1}{2}T_3 \wedge \tau}g(Z_{T_3 \wedge \tau})|Z_0 = z\right]$$

$$\leq \sup_{z: \ \|z-x\|=r_2} \mathbb{E}\left[e^{-\frac{1}{2}T_3}g_3\mathbb{I}_{T_3<\tau} + e^{-\frac{1}{2}\tau}\mathbb{I}_{T_3>\tau}|Z_0 = z\right]$$

On the other hand, applying the continuity of Brownian motion we have that $T_2 < \tau$ whenever Z_0 lies outside the ball of radius r_2, so

$$g_3 = \sup_{z: \ \|z-x\|=r_3} \mathbb{E}\left[e^{-\frac{1}{2}T_2}g(T_2)|Z_0 = z\right] \leq g_2$$

So in fact

$$g_3 \leq \sup_{z: \ \|z-x\|=r_2} \mathbb{E}\left[e^{-\frac{1}{2}T_3}\mathbb{I}_{T_3<\tau}g_3 + e^{-\frac{1}{2}\tau}\mathbb{I}_{T_3>\tau}|Z_0 = z\right]$$

$$g_3 \leq \frac{\sup_{z: \ \|z-x\|=r_2} \mathbb{E}\left[e^{-\frac{1}{2}\tau}\mathbb{I}_{T_3>\tau}|Z_0 = z\right]}{1 - \sup_{z: \ \|z-x\|=r_2} \mathbb{E}\left[e^{-\frac{1}{2}T_3}\mathbb{I}_{T_3<\tau}|Z_0 = z\right]} = L$$

To calculate this upper-bound L, defined above, Wendel gives explicit formulas (cf. [33]). We caution that in this document a somewhat nonstandard notation is used, namely Wendel uses $\mathbb{E}[A; B]$ to indicate $\mathbb{E}[A \times \mathbb{I}_B]$. For any z with $\|z - x\| = r_2$, Wendel uses the symmetry of the problem to show that

$$\mathbb{E}\left[e^{-\frac{1}{2}\tau}\mathbb{I}_{T_3>\tau}|Z_0 = z\right] = \left(\frac{r_1}{r_2}\right)^h \frac{I(r_3)K(r_2) - I(r_2)K(r_3)}{I(r_3)K(r_1) - I(r_1)K(r_3)}$$

$$\mathbb{E}\left[e^{-\frac{1}{2}\tau}\mathbb{I}_{T_3<\tau}|Z_0 = z\right] = \left(\frac{r_3}{r_2}\right)^h \frac{I(r_1)K(r_2) - I(r_2)K(r_1)}{I(r_1)K(r_3) - I(r_3)K(r_1)}$$

where $h = (n-2)/2$ and I, K denote the modified Bessel functions of order h. This leads to the following explicit formula for L.

$$L = \frac{\left(\frac{r_1}{r_2}\right)^h (I_3 K_2 - I_2 K_3)}{I_2 K_1 \left(\frac{I_3}{I_2} - \left(\frac{r_3}{r_2}\right)^h\right) + I_1 K_2 \left(\left(\frac{r_3}{r_2}\right)^h - \frac{K_3}{K_2}\right)} \tag{B1}$$

where we denote $I_1 = I(r_1), K_1 = K(r_1), I_2 = I(r_2)$, and so-on. To prove our result, it thus suffices to show we can drive L to zero by taking n sufficiently large.

The numerator of L in Equation (B1) converges to zero as $r_1 \to 0$, because $\frac{r_1}{r_2} \to 0, h > 0$ and the other terms are constant. On the other hand, the denominator explodes, because as $r_1 \to 0$ we have

$$\left(\frac{I_3}{I_2} - \left(\frac{r_3}{r_2}\right)^h\right) K_1 I_2 \to +\infty$$

$$\left(\left(\frac{r_3}{r_1}\right)^h - \frac{K_3}{K_2}\right) I_1 K_2 \to 0$$

These limits follow immediately from three properties of Bessel functions:

- $K(x) \to \infty, I(x) \to 0$ as $x \to 0$ for $h > 0$

- $K(x), I(x) > 0$ for $x > 0, h > 0$

- $\frac{I(y)}{I(x)} > \left(\frac{y}{x}\right)^h$ for $y > x$ and $h > 0$

The first two properties are well-known and can be found in DLMF (cf. [39]); the second can be found in Baricz (cf. [39, 40]). In conclusion, since the numerator vanishes and the denominator explodes, we have that overall L vanishes. Applying a Chernoff bound, we have our result for the case that $x \in \Omega$.

What happens if x is not in the closure of Ω? Then by taking r_1 sufficiently small we can ensure that $A \cap \Omega = \emptyset$, so $\tau = \infty$. Thus the result is proved automatically.

What if x is precisely on the boundary of Ω? Here we must use the smoothness of the boundary of Ω. By picking r_3 sufficiently small, the smoothness guarantees that Ω is arbitrarily well-approximated by a half-plane when restricted to a ball $\mathcal{B}(x, r_3)$. In this half-plane case, identical arguments to the ones above can be used to argue that we can always

take a r_1 that is yet smaller than r_3 and ensure that the hitting time is arbitrarily long. Finally, to account for the slight discrepancy between the half-plane case and the actual case for some finite r_3, we appeal to the continuity of the Poisson equation which governs g with respect to boundary condition (cf. [41]). □

Lemma 3. *Fix $0 < \epsilon$ and $0 < r_1 < r_3$. Then we can always find an n with the following property. Pick any open set $\Omega \in \mathbb{R}^n$, any x satisfying $\mathcal{B}(x, r_3) \subset \Omega$, and any $x_0 \notin \mathcal{B}(x, r_3)$. Consider a Brownian motion Z trapped inside Ω by reflecting boundaries and let τ denote the first hitting time of the process to $\mathcal{B}(x, r_1)$. Our choice of n guarantees that*

$$\mathbb{P}(\tau < 1/\epsilon | Z_t = x_0) \le \epsilon$$

Proof. Following the same arguments found in Lemma 2, we again obtain that $\mathbb{E}[e^{-\tau/2}|Z_0 = x_0]$ is bounded by

$$L = \frac{\left(\frac{r_1}{r_2}\right)^h (I_3 K_2 - I_2 K_3)}{I_2 K_1 \left(\frac{I_3}{I_2} - \left(\frac{r_3}{r_2}\right)^h\right) + I_1 K_2 \left(\left(\frac{r_3}{r_2}\right)^h - \frac{K_3}{K_2}\right)} \tag{B2}$$

To show our proof, it thus suffices to show we can drive this quantity to zero and then apply a Chernoff bound.

Let us first look at the numerator of L in Equation B1. Asymptotics from the DLMF give that as $h \to \infty$ we have

$$I(x) \sim \frac{x^h}{2^h \Gamma(h+1)} \qquad\qquad K(x) \sim \frac{2^h \Gamma(h+1)}{(2h)x^h}$$

Here by $f_1(h) \sim f_2(h)$ we mean "asymptotic equivalence," i.e. $\lim_{h\to\infty} f_1(h)/f_2(h) = 1$. Plugging these in, we see that both terms in the numerator are asymptotically vanishing.

Now let us turn to the denominator. Using the asymptotic formula above, we first note that

$$\left(\frac{r_3}{r_2}\right)^h I_1 K_2 \sim \frac{1}{2h}\left(\frac{r_3 r_1}{r_2^2}\right)^h = \frac{1}{2h} \to 0$$

$$-\frac{K_3}{K_2} I_1 K_2 \sim -\frac{1}{2h}\left(\frac{r_1}{r_3}\right)^h \to 0$$

So those terms are negligible. However, the other two terms of the denominator are in fact exploding: one to positive infinity and one to negative infinity. To understand this delicate balance, we these we turn to Lemma 4. Applying this Lemma and the asymptotics of the DLMF, we obtain that

$$
\left(\frac{I_3}{I_2} - \left(\frac{r_3}{r_2} \right)^h \right) K_1 I_2 \geq \frac{r_3^h}{\not{I_2}} \times \frac{r_3^2 - r_2^2}{2^{h+2}\Gamma(h+2)} K_1 \not{I_2}
$$

$$
\sim r_3^h \times \frac{r_3^2 - r_2^2}{2^{h+2}\Gamma(h+2)} \frac{2^h \Gamma(h+1)}{2hr_1^h}
$$

$$
= \left(\frac{r_3}{r_1} \right)^h \left(\frac{r_3^2 - r_2^2}{8h(h+1)} \right)
$$

which is indeed exploding to positive infinity as $h = (n-2)/2 \to \infty$.

Thus, since the numerator vanishes and the denominator explodes to positive infinity, we have that L vanishes as $n \to \infty$. $\qquad \square$

Lemma 4. *Let I denote the modified bessel function of the first kind of order h. If $a > b$ then*

$$
\frac{I(a)}{I(b)} - \left(\frac{a}{b} \right)^h \geq \frac{a^h}{I(b)} \times \frac{a^2 - b^2}{2^{h+2}\Gamma(h+2)}
$$

Proof. Recall that I may be defined as

$$
I(x) = \sum_{m=0}^{\infty} \frac{x^{h+2m}}{2^{h+2m}\Gamma(m+h+1)\Gamma(m+1)}
$$

Thus

$$
\frac{I(a)}{I(b)} - \left(\frac{a}{b} \right)^h = \frac{I(a)b^h - a^h I(b)}{b^h I(b)}
$$

$$
= \frac{a^h b^h \sum_{m=0}^{\infty} \frac{a^{2m}-b^{2m}}{2^{h+2m}\Gamma(m+h+1)\Gamma(m+1)}}{b^h I(b)}
$$

Since $a > b$, we have that $a^{2m} - b^{2m}$ is always positive. Thus we can get a lower bound by simply taking one of the terms. Choosing $m = 1$, we get our final result. $\qquad \square$

C.   Proof of Theorem 1

Let $A \subset \tilde{A} \subset \Omega, B \subset \tilde{B} \subset \Omega$. Let $\tilde{A}, \tilde{B}$ be disjoint and $h_{A,B}(x)$ ε-flat with respect to $\Omega \backslash (\tilde{A} \cup \tilde{B})$. We assume the set boundaries are all smooth.

Under these conditions, we will show we can use local capacities to get good approximations for $h_{A,B}(x)$ when $x \notin \tilde{A}, \tilde{B}$. To do so, our key idea is to uncover upper and lower bounds on the value of the Dirichlet form applied to this function, $\mathscr{E}(h_{A,B}, h_{A,B})$. We will see that these bounds can be understood in terms of local capacities, and the resulting inequalities will then yield our main result in the form of Theorem 1.

Lemma 5. *Let $S = \Omega \backslash (A \cup B)$. The Dirichlet form of $h_{A,B}$ on S can be upper-bounded in terms of the capacities:*

$$\mathscr{E}_S(h_{A,B}, h_{A,B}) \leqslant \frac{\mathrm{cap}(A, \tilde{A})\,\mathrm{cap}(B, \tilde{B})}{\mathrm{cap}(A, \tilde{A}) + \mathrm{cap}(B, \tilde{B})}$$

Proof. We recall from Appendix A that

$$\mathscr{E}_S(h_{A,B}, h_{A,B}) = \mathrm{cap}(A, \Omega \backslash B) \leq \mathscr{E}_S(u, u)$$

for any u with $u(\partial A) = 1, u(\partial B) = 0$. Thus, to prove an upper bound it suffices to find any such function for which we can calculate $\mathscr{E}(u, u)$. To this end, consider

$$u_c(x) \triangleq \begin{cases} (1-c)h_{A,\tilde{A}^c}(x) + c & \text{if } x \in \tilde{A} \\ c(1 - h_{B,\tilde{B}^c}(x)) & \text{if } x \in \tilde{B} \\ c & \text{otherwise} \end{cases}$$

These functions are well-suited to giving us upper bounds on $\mathscr{E}_S(h_{A,B}, h_{A,B})$. Indeed:

- $u_c(\partial A) = 1, u_c(\partial B) = 0$. In fact, u_c takes a constant value c outside of $\tilde{A}, \tilde{B}$, drops smoothly in $\tilde{B}$ to achieve 0 on ∂B, and rises smoothly in $\tilde{A}$ to achieve 1 on $\partial \tilde{A}$.

- Noting that u_c is written as a piecewise combination of hitting probability functions, we see that its Dirichlet form can be calculated in terms of capacities on local regions: $\mathscr{E}_S(u_c, u_c) = (1-c)^2 \mathrm{cap}(A, \tilde{A}) + c^2 \mathrm{cap}(B, \tilde{B})$.

Thus the u_c functions give us a practical way to calculate upper bounds:

$$\mathscr{E}_S(h_{A,B}, h_{A,B}) \leq (1 - c)^2 \operatorname{cap}(A, \tilde{A}) + c^2 \operatorname{cap}(B, \tilde{B})$$

This inequality holds for any value of c. To get the best bound, we can take derivatives to minimize the right hand side with respect to c. The result is

$$c^* = \frac{\operatorname{cap}(A, \tilde{A})}{\operatorname{cap}(A, \tilde{A}) + \operatorname{cap}(B, \tilde{B})}$$

Plugging this into the previous equation, we obtain our final result. $\qquad\square$

Lemma 6. *Let* $S = \Omega \backslash (A \cup B)$. *Let* $m = \frac{1}{2}(\sup_{x \notin \tilde{A}, \tilde{B}} h_{A,B}(x) + \inf_{x \notin \tilde{A}, \tilde{B}}(h_{A,B}(x)))$. *The Dirichlet form of* $h_{A,B}$ *can be lower-bounded in terms of* m *and the capacities:*

$$\mathscr{E}_S(h_{A,B}, h_{A,B}) \geq \left(1 - m - \frac{\varepsilon}{2}\right)^2 \operatorname{cap}(A, \tilde{A}) \mathbb{I}_{m \leq 1 - \frac{\varepsilon}{2}} + \left(m - \frac{\varepsilon}{2}\right)^2 \operatorname{cap}(B, \tilde{B}) \mathbb{I}_{m \geq \frac{\varepsilon}{2}}$$

Proof. Recall that $\mathscr{E}_S(h_{A,B}, h_{A,B})$ can be expressed as an integral over S. We decompose this into three integrals: one over $\tilde{A}$, one over $\Omega \backslash \tilde{A}, \tilde{B}$, and one over $\tilde{B}$.

$$\mathscr{E}_S(h_{A,B}, h_{A,B}) = \int_{\tilde{A} \backslash A} \|\sigma \nabla h_{A,B}\|^2 \rho(dx) + \int_{\tilde{B} \backslash B} \|\sigma \nabla h_{A,B}\|^2 \rho(dx) + \int_{\Omega \backslash \tilde{A}, \tilde{B}} \|\sigma \nabla h_{A,B}\|^2 \rho(dx)$$

Since the integrand is always positive, we can get a lower bound by simply ignoring the integral over $\Omega \backslash \tilde{A}, \tilde{B}$ and focusing on the integrals over $\tilde{A}, \tilde{B}$. The $\tilde{A}, \tilde{B}$ integrals can be lower-bounded using capacities.

For example, let us focus on the A integral. There are two different possibilities we must consider:

- If $m > 1 - \varepsilon/2$ we will simply note that the integral over the $\tilde{A}$ region is non-negative.

- If $m \leq 1 - \varepsilon/2$, then we define

$$u_A(x) \triangleq \frac{h_{A,B}(x) - m - \frac{\varepsilon}{2}}{1 - m - \frac{\varepsilon}{2}}$$

Note that $h_{A,B}(x) = 1$ for $x \in \partial A$ and the ε-flatness condition shows that $h_{A,B}(x) \leq m + \frac{\varepsilon}{2}$ for $x \in \partial \tilde{A}$. Thus $u_A(\partial A) \geq 1, u_A(\partial \tilde{A}) \leq 0$. Lemma 8 from Appendix E

may then be applied to yield that $\mathscr{E}_{\tilde{A}\backslash A}(u_A, u_A) \geq \mathrm{cap}(A, \tilde{A})$. We can thus obtain the bound

$$\int_{\tilde{A}\backslash A} \|\sigma \nabla h_{A,B}\|^2 \rho(dx) = \left(1 - m - \frac{\varepsilon}{2}\right)^2 \mathscr{E}_{\tilde{A}\backslash A}(u_A, u_A)$$

$$\geq \left(1 - m - \frac{\varepsilon}{2}\right)^2 \mathrm{cap}(A, \tilde{A})$$

Putting these two possibilities together, we obtain

$$\int_{\tilde{A}\backslash A} \|\sigma \nabla h_{A,B}\|^2 \rho(dx) \geq \left(1 - m - \frac{\varepsilon}{2}\right)^2 \mathrm{cap}(A, \tilde{A}) \mathbb{I}_{m \leq 1 - \frac{\varepsilon}{2}}$$

Applying the same ideas to the integral over $\tilde{B}$, we obtain our result. $\qquad\square$

We are now in a position to prove Theorem 1 from the main text:

Theorem 1. *Assume that $h_{A,B}(x)$ is ε-flat relative to $\Omega\backslash(\tilde{A} \cup \tilde{B})$. Then the first-passage probabilities can be well-approximated in terms of the target capacities:*

$$\sup_{x \notin \tilde{A}, \tilde{B}} \left| h_{A,B}(x) - \frac{\mathrm{cap}(A, \tilde{A})}{\mathrm{cap}(A, \tilde{A}) + \mathrm{cap}(B, \tilde{B})} \right| \leqslant \varepsilon + \sqrt{\varepsilon/2}$$

Proof. To simplify notation, let $\kappa_A = \mathrm{cap}(A, \tilde{A})$ and $\kappa_B = \mathrm{cap}(B, \tilde{B})$. Applying the previous two lemmas together, we obtain the inequality

$$\frac{\kappa_A \kappa_B}{\kappa_A + \kappa_B} \geq \mathscr{E}(h_{A,B}, h_{A,B}) \geq \left(1 - m - \frac{\varepsilon}{2}\right)^2 \kappa_A \mathbb{I}_{m \leq 1 - \frac{\varepsilon}{2}} + \left(m - \frac{\varepsilon}{2}\right)^2 \kappa_B \mathbb{I}_{m \geq \frac{\varepsilon}{2}}$$

where $m = \frac{1}{2}(\sup_{x \notin \tilde{A}, \tilde{B}} h_{A,B}(x) + \inf_{x \notin \tilde{A}, \tilde{B}}(h_{A,B}(x)))$. In analyzing this inequality, there are three possibilities to consider.

- If $m \in (\varepsilon/2, 1 - \varepsilon/2)$, the quadratic formula yields

$$m \geqslant \frac{\kappa_A}{\kappa_A + \kappa_B} + \frac{\frac{\varepsilon}{2}(\kappa_B - \kappa_A) - \sqrt{\kappa_A \kappa_B \varepsilon(2 - \varepsilon)}}{\kappa_A + \kappa_B}$$

$$m \leqslant \frac{\kappa_A}{\kappa_A + \kappa_B} + \frac{\frac{\varepsilon}{2}(\kappa_B - \kappa_A) + \sqrt{\kappa_A \kappa_B \varepsilon(2 - \varepsilon)}}{\kappa_A + \kappa_B}$$

Applying $\left|\frac{\kappa_B - \kappa_A}{\kappa_A + \kappa_B}\right| \leq 1$ and the fact that the geometric mean $\sqrt{\kappa_A \kappa_B}$ never exceeds the arithmetic mean $(\kappa_A + \kappa_B)/2$, it follows that

$$\left| m - \frac{\kappa_A}{\kappa_A + \kappa_B} \right| \leq \frac{\varepsilon + \sqrt{\varepsilon(2 - \varepsilon)}}{2}$$

Applying the fact that m was designed so that $|h_{A,B}(x) - m| < \varepsilon/2$ for all $x \notin \tilde{A}, \tilde{B}$, we obtain

$$\left| h_{A,B}(x) - \frac{\kappa_A}{\kappa_A + \kappa_B} \right| \leq \frac{2\varepsilon + \sqrt{\varepsilon(2 - \varepsilon)}}{2}$$

- If $m < \varepsilon/2$, our equations become

$$\frac{\cancel{\kappa_A}\kappa_B}{\kappa_A + \kappa_B} \geq \left(1 - m - \frac{\varepsilon}{2} \right)^2 \cancel{\kappa_A}$$

Our assumption that $m \leq \varepsilon/2$ indicates that $(1 - m - \varepsilon/2)^2 \geq (1 - \varepsilon)^2$, thus in fact we have

$$\frac{\kappa_B}{\kappa_A + \kappa_B} \geq (1 - \varepsilon)^2 = 1 + \varepsilon^2 - 2\varepsilon$$

which means that $\kappa_A/(\kappa_A + \kappa_B) \leq 2\varepsilon - \varepsilon^2 \leq 2\varepsilon$. Thus we assumed $m \in [0, \varepsilon/2]$ and showed that $\kappa_A/(\kappa_A + \kappa_B) \in [0, 2\varepsilon - \varepsilon^2]$, so it follows that

$$\left| m - \frac{\kappa_A}{\kappa_A + \kappa_B} \right| \leq 2\varepsilon - \varepsilon^2$$

and so for any $x \notin \tilde{A}, \tilde{B}$, we have

$$\left| h_{A,B}(x) - \frac{\kappa_A}{\kappa_A + \kappa_B} \right| \leq 2.5\varepsilon - \varepsilon^2$$

- If $m > 1 - \varepsilon/2$, the same bound can be achieved by arguments which are symmetric to those employed in $m < \varepsilon/2$:

$$\left| h_{A,B}(x) - \frac{\kappa_A}{\kappa_A + \kappa_B} \right| \leq 2.5\varepsilon - \varepsilon^2$$

Our final result is found by noting that all these bounds are upper-bounded by $\varepsilon + \sqrt{\varepsilon/2}$. $\quad\square$

D. Proof of Proposition 1

We first establish a lemma, using Green's first identity and some properties of the stationary SDE (1), under the reversibility conditions (3), relative to U:

Lemma 7. *Fix some $S \subset \Omega$ with smooth boundary. Then for any smooth function g that satisfies $\mathcal{L}g = 0$ and smooth function f,*

$$\int_S \nabla f(x)^T a(x) \nabla g(x) e^{-U(x)} dx = \int_{\partial S} f(x) \mathfrak{n}(x)^T a(x) \nabla g(x) e^{-U(x)} \mathscr{H}(dx)$$

where $\mathfrak{n}$ are the normal vectors facing out of the set S and $\mathscr{H}(dx)$ is the integral with respect to the $(n-1)$-dimensional Hausdorff measure and

$$(\mathcal{L}f)(x) \triangleq \sum_i b_i(x) \frac{\partial f(x)}{\partial x_i} + \frac{1}{2} \sum_{ij} a_{ij}(x) \frac{\partial^2 f(x)}{\partial x_i \partial x_j}$$

Proof. This result is essentially a direct corollary of Green's identities. Apply Green's first identity to get

$$\int_S \nabla f^T a \nabla g e^{-U} dx$$
$$= \int_{\partial S} f \mathfrak{n}^T a \nabla g e^{-U} \mathscr{H}(dx) - \int_S f \nabla \cdot (a \nabla g e^{-U}) dx$$

where

$$\nabla \cdot (a \nabla g e^{-U}) = \sum_i \frac{\partial}{\partial x_i} \left[\sum_j e^{-U} a_{ij} \frac{\partial g}{\partial x_j} \right]$$

Next, using the reversibility constraint on b from Equation (3), it's not hard to verify that

$$\nabla \cdot (a \nabla g e^{-U}) = 2 e^{-U} \mathcal{L} g = 0$$

This gives us the desired result. $\square$

Proposition 1. *For any regions G and $\tilde{G}$ having smooth boundaries and such that $A \subset$*

$G \subset \tilde{G} \subset \tilde{A}$, cap$(A, \tilde{A},)$ *can be expressed as a flux leaving* $\tilde{G}\backslash G$:

$$\text{cap}(A, \tilde{A}) = \int_{\partial(\tilde{G}\backslash G)} h_{A,\tilde{A}^c}(x)\mathfrak{n}(x)^T a(x)\nabla h_{G,\tilde{G}^c}(x)e^{-U(x)}\mathscr{H}(dx)$$

where $a(x) = \sigma(x)\sigma(x)^T$ *is the diffusion matrix,* $\mathscr{H}(dx)$ *is the* $(n-1)$*-dimensional Hausdorff measure, and* $\mathfrak{n}$ *represents the outward-facing (relative to* $\tilde{G}\backslash G$*) normal vector on* $\partial(\tilde{G}\backslash G)$.

Proof. This result is certainly known, but we include a proof here because we were unable to find a proof in the literature. First recall that $\mathcal{L}h_{A,\tilde{A}^c} = 0$ and

$$\text{cap}(A, \tilde{A}) = \int_{\tilde{A}\backslash A} \nabla h_{A,\tilde{A}^c}(x)^T a(x)\nabla h_{A,\tilde{A}^c}(x)e^{-U(x)}dx$$

Together with Lemma 7, this yields that

$$\text{cap}(A, \tilde{A}) = \int_{\partial(\tilde{A}\backslash A)} h_{A,\tilde{A}^c}\mathfrak{n}^T a\nabla h_{A,\tilde{A}^c}e^{-U}\mathscr{H}(dx) = -\int_{\partial A} \mathfrak{n}^T a\nabla h_{A,\tilde{A}^c}e^{-U}\mathscr{H}(dx) \qquad \text{(D1)}$$

where in the last step we used $h_{A,\tilde{A}^c}(x) = 1, x \in \partial A, h_{A,\tilde{A}^c}(x) = 0, x \in \partial\tilde{A}$. Also, note that the normal vector on the right hand side is pointing *out of* the set A, as is our convention. Hence then negative sign.

Next we apply Lemma 7 again to get

$$0 = \int_{G\backslash A} \nabla(1)a\nabla h_{A,\tilde{A}^c}^T e^{-U}dx = \int_{\partial(G\backslash A)} \mathfrak{n}^T a\nabla h_{A,\tilde{A}^c}e^{-U}\mathscr{H}(dx)$$

Combining this with Equation D1 gives us

$$\text{cap}(A, \tilde{A}) = -\int_{\partial A} \mathfrak{n}^T a\nabla h_{A,\tilde{A}^c}e^{-U}\mathscr{H}(dx) = \int_{\partial G} \mathfrak{n}^T a\nabla h_{A,\tilde{A}^c}e^{-U}\mathscr{H}(dx) \qquad \text{(D2)}$$

Using the facts that $h_{G,\tilde{G}^c}(x) = 1, x \in \partial G, h_{G,\tilde{G}^c}(x) = 0, x \in \partial\tilde{G}$, and $\mathcal{L}h_{G,\tilde{G}^c} = 0$, we apply

Lemma 7 two more times to obtain

$$\text{cap}(A, \tilde{A}) = \int_{\partial G} \mathfrak{n}^T a \nabla h_{A, \tilde{A}^c} e^{-U} \mathscr{H}(dx) = \int_{\partial G} h_{G, \tilde{G}^c} \mathfrak{n}^T a \nabla h_{A, \tilde{A}^c} e^{-U} \mathscr{H}(dx)$$

$$= \int_{\partial(\tilde{G} \backslash G)} h_{G, \tilde{G}^c} \mathfrak{n}^T a \nabla h_{A, \tilde{A}^c} e^{-U} \mathscr{H}(dx) = \int_{\tilde{G} \backslash G} \nabla h_{G, \tilde{G}^c} a \nabla h_{A, \tilde{A}^c} e^{-U} dx$$

$$= \int_{\partial(\tilde{G} \backslash G)} h_{A, \tilde{A}^c} \mathfrak{n}^T a \nabla h_{G, \tilde{G}^c} e^{-U} \mathscr{H}(dx)$$

$\square$

Corollary. *For any region S having smooth boundary ∂S, and such that $A \subset S \subset \tilde{A}$, $\text{cap}(A, \tilde{A},)$ can be expressed as a flux leaving S:*

$$\text{cap}(A, \tilde{A}) = \int_{\partial S} \mathfrak{n}(x)^T a(x) \nabla h_{A, \tilde{A}^c}(x) e^{-U(x)} \mathscr{H}(dx)$$

where a and $\mathscr{H}(dx)$ are as defined in the Proposition, and $\mathfrak{n}$ is the outward-facing normal on ∂S.

Proof. Put $G = S$ in Equation (D2). $\square$

E.   Inequality Boundary Conditions for the Variational Form

Recall that $h_{A,B}(x)$ may be defined variationally. We have let

$$\mathscr{E}(f, g) \triangleq \int_{\Omega} \nabla f(x)^T a(x) \nabla g(x) \rho(dx)$$

denote the "Dirichlet Form." Let $\Omega \subset \mathbb{R}^n$ compact and open with smooth boundary. Let $\mathscr{L}^2(\bar{\Omega}, \rho)$ denote the Hilbert space of functions on $\bar{\Omega}$ which are square-integrable with respect to a continuous positive measure $\rho(dx) = e^{-U} dx$. Let $\mathcal{H}^1(\bar{\Omega}, \rho) = W^{1,2}(\bar{\Omega}, \rho) \subset \mathscr{L}^2(\bar{\Omega}, \rho)$ denote the corresponding once-weakly-differentiable Hilbert Sobolev space. Let $A, B \subset \Omega$, open, disjoint, with smooth boundary, and define $\text{cap}(A, \Omega \backslash B) \in \mathbb{R}$ as the minimizing value

of the problem

$$\min_{u \in \mathcal{H}^1} \quad \mathscr{E}(u, u)$$

$$\text{subject to} \quad u(x) = 1, x \in A$$

$$u(x) = 0, x \in B$$

It is natural to consider an apparently different problem, where the equality boundary conditions are replaced with inequalities. Here we show that it is not possible to get lower than $\text{cap}(A, \Omega \backslash B)$ by such a relaxation.

Lemma 8. *Let $\tilde{h}$ satisfy $\tilde{h}(x) \geq 1$ on A and $\tilde{h}(x) \leq 0$ on B. Then $\mathscr{E}(\tilde{h}, \tilde{h}) \geq \text{cap}(A, \Omega \backslash B)$.*

Proof. This result is certainly known, but we include a proof here because we were unable to find a proof in the literature. Let $k = \texttt{clamp}(\tilde{h}, 0, 1)$, i.e.

$$k(x) = \begin{cases} \tilde{h}(x) & \tilde{h}(x) \in [0, 1] \\ 0 & \tilde{h}(x) \leq 0 \\ 1 & \tilde{h}(x) \geq 1 \end{cases}$$

Note that $k \in \mathcal{H}^1$ and satisfies the equality boundary conditions. Thus, by definition, $\text{cap}(A, \Omega \backslash B) \leq \mathscr{E}(k, k)$. This immediately yields our result:

$$\text{cap}(A, \Omega \backslash B) \leq \mathscr{E}(k, k) = \int \|\sigma \nabla k\|^2 \rho(dx)$$

$$= \int_{x:\ \tilde{h}(x) \in [0,1]} \|\sigma \nabla \tilde{h}\|^2 \rho(dx)$$

$$\leq \int \|\sigma \nabla \tilde{h}\|^2 \rho(dx) = \mathscr{E}(\tilde{h}, \tilde{h})$$

$\square$

F.   Shell Method

The algorithm for estimating local hitting probabilities is outlined as follows:

Algorithm 1. *Estimating $h_{R,\tilde{R}^c}(x)$ for many values of x on a shell ∂S*

Input: $R \subset S \subset \tilde{R} \subset \Omega$ and a stationary reversible diffusion process $\{X_t\}_{t\geq 0}$ in Ω with invariant measure $\mu = e^{-U(x)}\mathrm{d}x$. We also require a series of subsets

$$R = S_0 \subset S_1 \subset \cdots \subset S_{m-1} \subset S_m = S \subset S_{m+1} \subset \cdots \subset S_n = \tilde{R}$$

which indicate a kind of reaction coordinate.

Output: A collection of points $z_1, \cdots z_{N_p}$ on ∂S sampled from the invariant measure $\mu = e^{-U(x)}\mathrm{d}x$ restricted on ∂S, along with estimates of $h_{R,\tilde{R}^c}(z_i)$ for each point.

1. *Discretize the space.*

   (a) *Generate an ensemble of samples $z_1, \ldots, z_{N_p}$ on ∂S according to the invariant measure $\mu = e^{-U(x)}\mathrm{d}x$ restricted to ∂S.*

   (b) *Evolve the ensemble on ∂S, by repeatedly sampling an initial location from the uniform distribution on $\{z_1, \ldots, z_{N_p}\}$ and carry out a local simulation following the dynamics of $\{X_t\}_{t\geq 0}$ until the trajectory hits either ∂S_{m-1} or ∂S_{m+1}. Record the hitting locations on ∂S_{m-1} and ∂S_{m+1} until we have N_p points on both ∂S_{m-1} and ∂S_{m+1}. In most cases, the process is more likely to hit one of S_{m-1}, S_{m+1} than the other, and we need to run more than $2N_p$ local simulations to get at least N_p samples on both shells. We store the results of the redundant local simulations for future estimation of transition probabilities.*

   (c) *Repeat the above process to sequentially evolve the ensembles on $\partial S_{m-1}, \ldots, \partial S_2$ and on $\partial S_{m+1}, \ldots, \partial S_{n-2}$, to get N_p samples on all of the intermediate shells $\partial S_1, \ldots, \partial S_{n-1}$. Store the results of the redundant local simulations for future estimation of transition probabilities.*

   (d) *For each one of the shells $\partial S_1, \ldots, \partial S_{n-1}$, cluster the N_p samples on that shell into N_b states. In our implementation, we use k-means, and represent the N_b states by the N_b centroids we get from the algorithm.*

   The result of this step is a partitioning of each shell ∂S_i into N_b regions, representing an adaptive discretization of the shells. For a point on a shell ∂S_i, we identify its corresponding discrete state by finding the nearest centroid.

2. *Estimate the transition probabilities between these discrete states by running an additional N_s local simulations for each one of the N_b states on each shell. The result of this step is an estimate of the probability of transitioning from state k on ∂S_i to state l on ∂S_j, which we denote by $P_{k,l}^{(i,j)}$, where $k, l \in \{1, \ldots, N_b\}$ and $i, j \in \{1, \ldots, n-1\}$ with $|i - j| = 1$.*

3. *Use the transition probabilities to get an estimate of the hitting probabilities for the N_b states on ∂S. In line with related works on Markov state models,[21–23] we approximate the continuous dynamics using closed-form calculations from the discrete Markov chain we have developed in the previous two steps. In particular, we estimate overall hitting probabilities using the standard "one-step analysis." For any $k \in \{1, \ldots, N_b\}$ and $i \in \{1, \ldots, n-1\}$, let $u_k^{(i)}$ denote the probability of hitting $\partial R = \partial S_0$ before hitting $\partial \tilde{R} = \partial S_n$ if we start the discretized process at state k on ∂S_i. We can calculate our object of interest by solving the matrix difference equation*

$$u^{(i)} = P^{(i,i+1)}u^{(i+1)} + P^{(i,i-1)}u^{(i-1)}, i = 1, \ldots, n-1$$

with boundary conditions $u^{(0)} = \mathbf{1}, u^{(n)} = \mathbf{0}$, where $\mathbf{0}$ and $\mathbf{1}$ are vectors of all 0's and 1's. This gives the estimated hitting probability for each discrete state. We then estimate the hitting probability of each point z_i by

$$h_{R,\tilde{R}^c}(z_i) = u_k^{(m)}, z_i \in state\ k\ on\ \partial S \tag{F1}$$

G. Details on Energy Function

For the energy function, we hand-designed two different kinds of landscape: random well energy, which we use for the region around target A, and random crater energy, which we use for the region around target B. The basic components of these energy functions are the well component, given by

$$F_w(x|d_w, r) = -\frac{d_w}{r^4}(||x - x_A||_2^4 - 2r^2||x - x_A||_2^2) - d_w \tag{G1}$$

where d_w gives the depth of the well; the crater component, given by

$$F_c(x|d_c, h, r) = \frac{d_c}{3b^2r^4 - r^6}(2||x - x_B||_2^2 - 3(b^2 + r^2)||x - x_B||_2^4 + 6b^2r^2||x - x_B||_2^2) - d_c \quad \text{(G2)}$$

where d_c and h give the depth and the height of the crater, respectively, and

$$b^2 = -\frac{1}{3d}(-3d_c r^2 + C + \frac{\Delta_0}{C}) \quad \text{(G3)}$$

with

$$C = 3r^2 \sqrt[3]{d_c h(d_c + \sqrt{d_c(d_c + h)})}$$
$$\Delta_0 = -9d_c h r^4$$

and finally a random component, given by

$$F_r(x|\mu, \sigma) = \sum_{i=1}^{m} \prod_{j=1}^{d} exp(-\frac{(x_j - \mu_{ij})^2}{2\sigma_{ij}^2}) \quad \text{(G4)}$$

where $\mu = (\mu_{ij})_{m \times d}$ and $\sigma = (\sigma_{ij})_{m \times d}$, with $\mu_i = (\mu_{i1}, \cdots, \mu_{i,d}), i = 1, \cdots, m$ being the locations of m Gaussian random bumps in the region around the targets, and $\sigma_{ij}, i = 1, \cdots, m, j = 1, \cdots, d$ gives the corresponding standard deviations.

To make sure the energy function is continuous, and the different components of the energy function are balanced, we introduce a mollifier, given by

$$F_m(x|x_0, r) = exp(-\frac{r}{r - ||x - x_0||_2^{20}}) \quad \text{(G5)}$$

where $x_0 = x_A, r = r_{\dot{A}}$ or $x_0 = x_B, r = r_{\dot{B}}$, depending on which target we are working with, and a rescaling of the random component, which is given by $0.1 * d_w$ if we are perturbing the well component, and $0.1 * (d_c + h)$ if we are perturbing the crater component.

Intuitively, for the well component, we use a 4th order polynomial to get a well-like energy landscape around the target that is continuous and differentiable at the boundary. Similarly, for the crater component, we use a 6th order polynomial to get a crater-like energy landscape around the target that is also continuous and differentiable at the boundary. For

the random component, we are essentially placing a number of Gaussian bumps around the target. And for the mollifier, we are designing the function such that it's almost exactly 1 around the target, until it comes to the outer boundary, when it transitions smoothly and swiftly to 0. To summarize, given parameters d_w, d_c, h and random bumps μ_A, μ_B with $\mu_i^A \in \dot{A} \setminus A, i = 1, \cdots, m_A, \mu_i^B \in \dot{B} \setminus B, i = 1, \cdots, m_B$, and the corresponding standard deviations σ^A, σ^B with $\sigma_{ij}^A, i = 1, \cdots, m_A, j = 1, \cdots, d, \sigma_{ij}^B, i = 1, \cdots, m_B, j = 1, \cdots, d$, the energy function we used in the experiments is given by

$$F(x) = F_w(x|d_w, r_{\dot{A}}) + 0.1 \times d_w \times F_m(x|x_A, r_{\dot{A}}) + F_r(x|\mu^A, \sigma^A), \forall x \in \dot{A} \setminus A \tag{G6}$$

$$F(x) = F_c(x|d_c, h, r_{\dot{B}}) + 0.1 \times (d_c + h) \times F_m(x|x_B, r_{\dot{B}}) + F_r(x|\mu^B, \sigma^B), \forall x \in \dot{B} \setminus B \tag{G7}$$

---

[1] H. A. Scheraga, M. Khalili, and A. Liwo, Annu. Rev. Phys. Chem. **58**, 57 (2007).

[2] A. Hospital, J. R. Goñi, M. Orozco, and J. L. Gelpí, Adv. Appl. Bioinform. Chem. **8**, 37 (2015).

[3] H. Lei, B. Caswell, and G. E. Karniadakis, Physical Review E **81**, 026704 (2010).

[4] V. Sotiropoulos and Y. N. Kaznessis, Chemical engineering science **66**, 268 (2011).

[5] D. T. Gillespie, The Journal of Chemical Physics **113**, 297 (2000).

[6] D. Holcman and Z. Schuss, Journal of Statistical Physics **117**, 975 (2004).

[7] W. E. and E. Vanden-Eijnden, J. Stat. Phys. **123**, 503 (2006).

[8] E. B. Baum, Phys. Rev. Lett. **57**, 2764 (1986).

[9] L. T. Wille, Phys. Rev. Lett. **59**, 372 (1987).

[10] J. Machta, Phys. Rev. E **80**, 056706 (2009).

[11] M. Christen and W. F. van Gunsteren, J. Comput. Chem. Computer Simu, **29**, 157 (2008).

[12] R. Samson and J. M. Deutch, J. Chem. Phys. **67**, 847 (1977), https://doi.org/10.1063/1.434853.

[13] J. M. Deutch, B. U. Felderhof, and M. J. Saxton, J. Chem. Phys. **64**, 4559 (1976), https://doi.org/10.1063/1.432088.

[14] A. F. Cheviakov, M. J. Ward, and R. Straube, Multiscale Modeling & Simulation **8**, 836 (2010).

[15] X. Li, Journal of Physics A: Mathematical and Theoretical **47**, 505202 (2014).

[16] C. Chevalier, O. Bénichou, B. Meyer, and R. Voituriez, J. Phys. A: Math. Theor. **44**, 025002 (2010).

[17] S. Condamin and O. Bénichou, J. Chem. Phys. **124**, 206103 (2006).

[18] D. Coombs, R. Straube, and M. Ward, SIAM J. Appl. Math. **70**, 302 (2009), https://doi.org/10.1137/080733280.

[19] A. E. Lindsay, A. J. Bernoff, and M. J. Ward, Multiscale Model. Simul. **15**, 74 (2017), https://doi.org/10.1137/16M1077659.

[20] J. Kaye and L. Greengard, arXiv preprint arXiv:1906.04209 (2019).

[21] V. S. Pande, K. Beauchamp, and G. R. Bowman, Methods **52**, 99 (2010).

[22] J. D. Chodera and F. Noé, Curr. Opin. Struct. Biol. **25**, 135 (2014).

[23] B. E. Husic and V. S. Pande, J. Am. Chem. Soc. **140**, 2386 (2018).

[24] G. J. Moro, The Journal of chemical physics **103**, 7514 (1995).

[25] J. M. Bello-Rivas and R. Elber, J. Chem. Phys. **142**, 094102 (2015).

[26] P. Májek and R. Elber, J. Chem. Theory Comput. **6**, 1805 (2010).

[27] P.-L. Lions and A.-S. Sznitman, Communications on Pure and Applied Mathematics **37**, 511 (1984).

[28] Z.-Q. Chen, Probability theory and related fields **94**, 281 (1993).

[29] A. Bovier and F. den Hollander, *Metastability: A Potential-Theoretic Approach* (Springer, 2016).

[30] A. Bovier, M. Eckhoff, V. Gayrard, and M. Klein, J. Eur. Math. Soc. **6**, 399 (2004).

[31] A. M. A. West, R. Elber, and D. Shalloway, J. Chem. Phys. **126**, 145104 (2007).

[32] D. Aristoff, J. Bello-Rivas, and R. Elber, Multiscale Model. Simul. **14**, 301 (2016).

[33] J. G. Wendel, Ann. Probab. **8**, 164 (1980).

[34] N. H. Bingham, Zeitschrift für Wahrscheinlichkeitstheorie und Verwandte Gebiete **22**, 169 (1972).

[35] G. M. Lieberman, Journal of Mathematical Analysis and Applications **113**, 422 (1986).

[36] Z.-Q. Chen and M. Fukushima, *Symmetric Markov processes, time change, and boundary theory (LMS-35)*, Vol. 35 (Princeton University Press, 2012).

[37] H. Dret and B. Lucquin, *Partial Differential Equations: Modeling, Analysis and Numerical Approximation*, International Series of Numerical Mathematics (Springer International Pub-

lishing, 2016).

[38] J. Loper, Journal of Theoretical Probability (2018), 10.1007/s10959-018-0848-7.

[39] "NIST digital library of mathematical functions," `http://dlmf.nist.gov/`.

[40] Á. Baricz, Proceedings of the Edinburgh Mathematical Society **53**, 575 (2010).

[41] G. Strang, Numerische Mathematik **19**, 81 (1972).